Chapter 6

Transportation of micro-polar fluids by means of peristaltic waves of dilating amplitude in a tube of exponentially changing cross-sectional area: Application to sliding hiatus hernia

The contents of this chapter have been published in **Zeitschrift für Angewandte Mathematik und Mechanik**, **102**(4), (2022)1-24 .

6.1 Introduction

Hiatus hernia is a state when the upper part of the stomach slides up above the hiatus at a time the oesophagus contracts and then stays there with a little bit bulging (Figure 6.1). Hiatus is an opening in the diaphragm which is a dome shaped muscle lying between the chest and the abdomen. The oesophagus passes through the hiatus to join the stomach. The lower oesophageal sphincter, together with the crural diaphragm creates a high-pressure zone which functions as an anti-reflux barrier to provide protection from the caustic gastric content. For a short while, the lower oesophageal sphincter relaxes to allow passage of foodstuff into the abdomen (Boeckxstaens (2005)). Kahrilas *et al.* (1999) concluded that the hiatus hernia reduces the lower oesophageal sphincter pressure and alters its dynamic responsiveness by separating pressure components derived from the intrinsic lower oesophageal sphincter and extrinsic compression of the oesophagus in the hiatus canal. One of the possibilities, speculated so far, for hernia is shortening of the oesophagus, which pulls the oesophago-gastric junction up above the hiatus (Christensen and Miftakhov (2000)).

There are several related dysfunctions of oesophagus, for example, achalasia, gastro-oesophageal reflux disease etc. (Kahrilas *et al.* (1999); Carlson *et al.* (2018). Achalasia is a condition in which the muscles of the lower part of oesophagus fail to relax. Carlson *et al.* (2018) studied and reported that the purpose of achalasia treatment is to improve patient symptoms and to reduce oesophageal detention but also recommended further studies. This achalasia may cause hiatus hernia as speculated by Christensen and Miftakhov (2000). Weyenberg (2013) studied diagnosis and grading of sliding hiatal hernia and reported uncertainty in the endoscopic diagnosis of hiatal hernia. Hence, clear endoscopic images are required in documenting endoscopic findings.

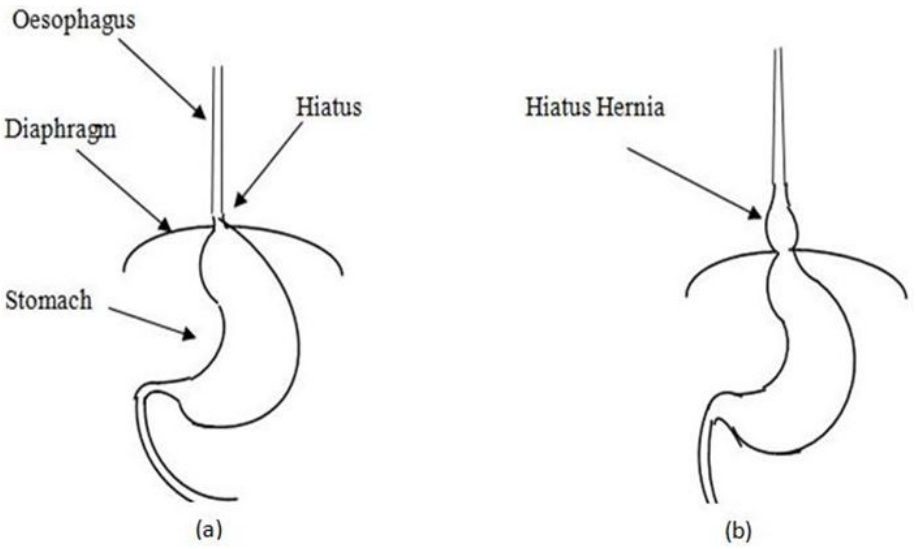

Figure 6.1: Diagrams for (a) Normal oesophagus and (b) Oesophagus suffering from sliding hiatus hernia (Figure 6.1 is taken from Pandey and Singh (2019)).

Pandey *et al*. (2017) studied variation of pressure from cervical to the distal end of oesophagus during swallowing of food bolus. Their assumption of waves with increasing amplitude, based on anatomical data produced by Xia *et al*. (2009), endorsed the experimental outcome of Kahrilas *et al*. (1995) of higher pressure in the distal part of the oesophagus required for swallowing of food boluses which become gradually globular while traversing the journey from the phyrangeal to the cardiac sphincter. Following this, several modifications to previous investigations on non-Newtonian fluids were reported (Pandey and Tiwari (2017), Pandey and Singh (2018), Pandey and Tiwari (2020), Pandey and Chandra (2020)).

Pandey and Singh (2019) studied a model of peristaltic transport of Herschel–Bulkley fluids in tubes of variable cross-section for studying sliding hiatus hernia. Waves that propagate along the tube wall had amplitude increasing exponentially. They concluded that the difference between the lower and the upper oesophageal pressure decreases if the tube diverges because less pressure is

enough to transport the fluid. Even if merely the lower portion of the cylindrical tube diverges, they observed that pressure lowers right from the beginning. Experimental observations endorse this. This is experienced when oesophagus suffers from sliding hiatus hernia causing the lower oesophagus to bulge towards the end. In contrast to this, if the lower part of the tube subsequently converges towards the end after divergence, pressure is found to increase. Pressure is also found to increase with the flow behavior index. When the bolus is nearing the cardiac sphincter, pressure-rise and pressure-drop are both less in a diverging tube than that in a uniform tube. Therefore, the pressure required to cross the cardiac sphincter is less if oesophagus diverges.

Oesophageal cross section does not remain uniform at least at the distal end when it relaxes from contraction under herniation; or it may swell at the lower end with an altered shape throughout, may be along the entire length. Pandey and Singh (2019) who studied peristaltic transport of Herschel–Bulkley fluids in tubes of variable cross-sections followed previous considerations of cross sectional variations and assumed to be linear (Mekheimer and El-Kot (2008, 2004), Mekheimer (2002)).

Micro-polar fluid has no similarity with this; it neither possesses flow behaviour index, nor does it have any plug flow region. The micro constituents of micro-polar fluids undergo rotation and the presence of micro constituents makes them a different non-Newtonian fluid (cf. Grzegorz Lukaszewicz (1999)). Therefore, it requires a separate analysis.

Solutions of roasted cereal powders, blood, chyme, polymer solutions, colloidal solutions, drilling fluids in oil industries etc may be considered micro-polar type (Bourne (2002), Pandey and Tripathi (2011). Peristaltic transport of micro-polar fluids has been studied under various conditions by several researchers

[Pandey and Tripathi (2011), Mekheimer (2008)]. Pandey and Tripathi (2011) had investigated the flow of micro-polar fluids in a finite length channel tube, the results of which were improved in light of the investigations [Pandey *et al.* (2017)] for cylindrical flow by Pandey and Chandra (2020). Chandra and Pandey (2018) further modelled peristaltic transport of micro-polar fluids by considering linear divergence of a herniated oesophagus following Pandey and Singh (2019). However, this does not seem to be very appropriate model for herniated oesophagus. This appears to be a crude approximation to match the altered shape of the oesophagus when the abdomen has protruded up through the hiatus. An exponential curve seems to more suitably fit the shape by the curve fitting techniques.

Hence, we prefer to consider an exponential growth to match shape-deformation.

This discussion leads to the formulation of the following problem:

6.2 Problem Formulation

Let us consider the transport of a micro-polar fluid in tube of length $\tilde{l}$, which is cylindrical in shape with circular cross section. The motion is created by continuous peristaltic waves of contraction that advance along the wall of the tube (Figure 6.2) given by

$$\tilde{h}(\tilde{x}, \widetilde{\omega}, \tilde{t}) = ae^{\tilde{b}\tilde{x}} - \widetilde{\phi}e^{\widetilde{\omega}\tilde{x}}\cos^2\frac{\pi}{\lambda}(\tilde{x} - c\tilde{t}), \tag{6.1}$$

where $\tilde{h}$, $\tilde{x}$, $\tilde{t}$, a, $\tilde{b}$, $\widetilde{\phi}$, λ, $\widetilde{\omega}$ and c respectively denote for the radial displacement of the wall, the axial coordinate, time, the radius of the tube, the gradient parameter, the initial amplitude of the wave, the wavelength, wave amplitude dilation parameter and the wave velocity. The gradient parameter determines the deformation of the tube or the oesophagus due to herniation while the wave amplitude dilation parameter quantifies the rate at which the wavelength increases.

Equations governing the motion of micro-polar fluids, by neglecting body forces and body couple, are given by

$$\frac{\partial \tilde{u}}{\partial \tilde{x}} + \frac{1}{\tilde{r}}\left(\frac{\partial(\tilde{r}\tilde{v})}{\partial \tilde{r}}\right) = 0, \tag{6.2}$$

$$\rho\left(\frac{\partial \tilde{u}}{\partial \tilde{t}} + \tilde{u}\frac{\partial \tilde{u}}{\partial \tilde{x}} + \tilde{v}\frac{\partial \tilde{u}}{\partial \tilde{r}}\right) = -\frac{\partial \tilde{p}}{\partial \tilde{x}} + k\frac{1}{\tilde{r}}\frac{\partial(\tilde{r}\tilde{w})}{\partial \tilde{r}} + (\mu + k)\left(\frac{\partial^2 \tilde{u}}{\partial \tilde{x}^2} + \frac{1}{\tilde{r}}\frac{\partial}{\partial \tilde{r}}\left(\tilde{r}\frac{\partial \tilde{u}}{\partial \tilde{r}}\right)\right), \tag{6.3}$$

$$\rho\left(\frac{\partial \tilde{v}}{\partial \tilde{t}} + \tilde{u}\frac{\partial \tilde{v}}{\partial \tilde{x}} + \tilde{v}\frac{\partial \tilde{v}}{\partial \tilde{r}}\right) = -\frac{\partial \tilde{p}}{\partial \tilde{r}} - k\frac{\partial \tilde{w}}{\partial \tilde{x}} + (\mu + k)\left(\frac{\partial^2 \tilde{v}}{\partial \tilde{x}^2} + \frac{\partial}{\partial \tilde{r}}\left(\frac{1}{\tilde{r}}\frac{\partial(\tilde{r}\tilde{v})}{\partial \tilde{r}}\right)\right), \tag{6.4}$$

$$\rho\widetilde{\sigma}\left(\frac{\partial \tilde{w}}{\partial \tilde{t}} + \tilde{u}\frac{\partial \tilde{w}}{\partial \tilde{x}} + \tilde{v}\frac{\partial \tilde{w}}{\partial \tilde{r}}\right) = -2k\tilde{w} + k\left(\frac{\partial \tilde{v}}{\partial \tilde{x}} - \frac{\partial \tilde{u}}{\partial \tilde{r}}\right) + \gamma\left(\frac{\partial^2 \tilde{w}}{\partial \tilde{x}^2} + \frac{\partial}{\partial \tilde{r}}\left(\frac{1}{\tilde{r}}\frac{\partial(\tilde{r}\tilde{w})}{\partial \tilde{r}}\right)\right) + (\alpha + \beta + \gamma)\widetilde{\nabla}\left(\widetilde{\nabla}.\tilde{w}\right). \tag{6.5}$$

where $\tilde{u}$, $\tilde{v}$, $\tilde{w}$, $\tilde{r}$, ρ, $\widetilde{\sigma}$ are respectively denote the axial and radial velocities, the micro-polar vector, the radial coordinate, the fluid density, the micro-gyration parameter; and μ, k, α, β, γ represent respectively the material constants constrained as given below:

$$2\mu + k \geq 0, \quad k \geq 0, \quad 3\alpha + \beta + \gamma \geq 0, \quad \gamma \geq \left|\beta\right|. \tag{6.6}$$

The following the non-dimensional parameters being introduced for subsequent analyses:

$$x = \frac{\tilde{x}}{\lambda}, \quad r = \frac{\tilde{r}}{a}, \quad t = \frac{c\tilde{t}}{\lambda}, \quad u = \frac{\tilde{u}}{c}, \quad v = \frac{\tilde{v}}{c\delta}, \quad \delta = \frac{a}{\lambda}, \quad w = \frac{a\tilde{w}}{c}, \quad h = \frac{\tilde{h}}{a}, \quad b = \tilde{b}\lambda, \quad l = \frac{\tilde{l}}{\lambda},$$
$$\phi = \frac{\widetilde{\phi}}{a}, \quad \sigma = \frac{\widetilde{\sigma}}{a^2}, \quad p = \frac{\tilde{p}a^2}{\mu c\lambda}, \quad Re = \frac{\rho ca\delta}{\mu}, \quad Q = \frac{\tilde{Q}}{\pi a^2 c}, \quad \omega = \widetilde{\omega}\lambda. \tag{6.7}$$

where $\delta = \frac{a}{\lambda}$ is the wave number; Re the Reynolds number and Q the volume flow rate.

Equations (6.2)-(6.5), in terms of the non-dimensional parameters, reduce to

$$\frac{\partial u}{\partial x} + \frac{1}{r}\left(\frac{\partial (rv)}{\partial r}\right) = 0, \tag{6.8}$$

$$Re\delta\left(\frac{\partial u}{\partial t} + u\frac{\partial u}{\partial x} + v\frac{\partial u}{\partial r}\right) = -\frac{\partial p}{\partial x} + \frac{N}{1-N}\frac{1}{r}\frac{\partial (rw)}{\partial r} + \frac{1}{1-N}\left(\delta^2\frac{\partial^2 u}{\partial x^2} + \frac{1}{r}\frac{\partial}{\partial r}\left(r\frac{\partial u}{\partial r}\right)\right), \tag{6.9}$$

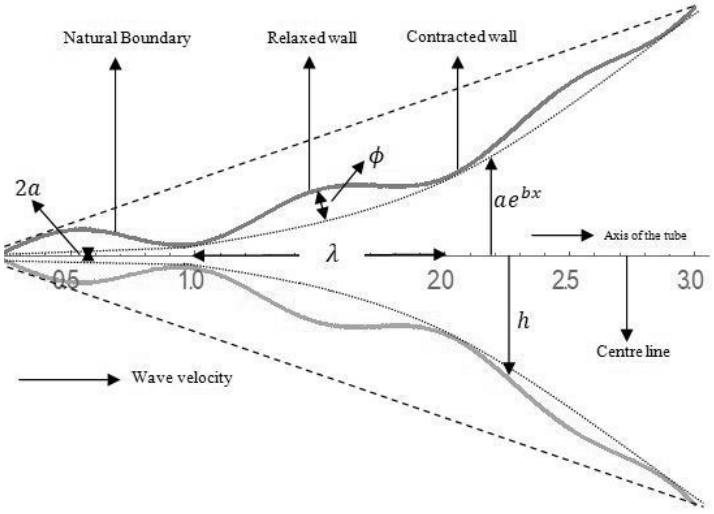

Figure 6.2: Schematic diagram (based on equation 6.16) of the flow under peristaltic waves of progressively dilating amplitude in an exponentially diverging tube.

$$Re\delta^3\left(\frac{\partial v}{\partial t}+u\frac{\partial v}{\partial x}+v\frac{\partial v}{\partial r}\right)=-\frac{\partial p}{\partial r}+\frac{\delta^2}{1-N}\left(-N\frac{\partial w}{\partial x}+\frac{\partial}{\partial r}\left(\frac{1}{r}\frac{\partial(rv)}{\partial r}\right)+\delta^2\frac{\partial^2 v}{\partial x^2}\right), \quad (6.10)$$

$$\frac{\sigma Re\delta(1-N)}{N}\left(\frac{\partial w}{\partial t}+u\frac{\partial w}{\partial x}+v\frac{\partial w}{\partial r}\right)=-2w+\left(\delta^2\frac{\partial v}{\partial x}-\frac{\partial u}{\partial r}\right)+\frac{2-N}{m^2}\left(\frac{\partial}{\partial r}\left(\frac{1}{r}\frac{\partial(rw)}{\partial r}\right)+\delta^2\frac{\partial^2 w}{\partial x^2}\right). \quad (6.11)$$

We apply the long wavelength and low Reynolds number approximations to reduces equations (6.8)-(6.11) to

$$\frac{\partial u}{\partial x}+\frac{1}{r}\left(\frac{\partial(rv)}{\partial r}\right)=0, \quad (6.12)$$

$$\frac{\partial p}{\partial x} = \frac{1}{1-N}\left\{\frac{N}{r}\frac{\partial (rw)}{\partial r} + \frac{1}{r}\frac{\partial}{\partial r}\left(r\frac{\partial u}{\partial r}\right)\right\}, \tag{6.13}$$

$$\frac{\partial p}{\partial r} = 0, \tag{6.14}$$

$$2w + \frac{\partial u}{\partial r} - \frac{2-N}{m^2}\frac{\partial}{\partial r}\left(\frac{1}{r}\frac{\partial (rw)}{\partial r}\right) = 0. \tag{6.15}$$

where $N = \frac{k}{(\mu+k)}$ is the coupling number which is a measure of particle coupling with its surroundings $(0 \leq N \leq 1)$, $m = \sqrt{\frac{a^2 k\,(2\mu+k)}{\gamma\,(\mu+k)}}$ is the micro-polar parameter and α, β do not appear in the governing as the micro-rotation vector is solenoidal, i.e. $\overrightarrow{\nabla} w = 0$.

The wall equation in the dimensionless form is

$$h(x,\omega,t) = e^{bx} - \phi e^{\omega x}\cos^2\pi (x-t), \tag{6.16}$$

The following are the boundary conditions to be applied on the governing equations subject to which the governing equations are to be solved in order to model the problem:

$$u(x,r,t)|_{r=h} = 0, \quad v(x,r,t)|_{r=h} = \frac{\partial h}{\partial t},$$

$$v(x,r,t)|_{r=0} = 0, \quad \frac{\partial u(x,r,t)}{\partial r}|_{r=0} = 0, \tag{6.17}$$

$$w(x,r,t)|_{r=0}= 0, \quad w(x,r,t)|_{r=h}= 0. \tag{6.18}$$

6.3 Mathematical Analysis

We integration equation (6.13), with respect to r yields

$$\frac{\partial u}{\partial r} = (1-N)\frac{r}{2}\frac{\partial p}{\partial x} - Nw + \frac{C_1}{r}. \tag{6.19}$$

where C_1 is an arbitrary function independent of r.

Using equation (6.19), equation (6.15) may be rearranged as

$$\frac{\partial^2 w}{\partial r^2} + \frac{1}{r}\frac{\partial w}{\partial r} - \left(m^2 + \frac{1}{r^2}\right)w = \frac{m^2}{2-N}\left\{(1-N)\frac{r}{2}\frac{\partial p}{\partial x} + \frac{C_1}{r}\right\}.$$

with the following general solution:

$$w = C_2 I_1(mr) + C_3 K_1(mr) - \frac{1}{2-N}\left\{(1-N)\frac{r}{2}\frac{\partial p}{\partial x} + \frac{C_1}{r}\right\}. \tag{6.20}$$

where C_2, C_3 are also arbitrary functions independent of r and $I_1(mr)$ $K_1(mr)$ are respectively modified Bessel functions of the 1^{st} and 2^{nd} kind of the 1^{st} order.

Equation (6.20) is solved subject to the second condition of (6.18) and first condition of (6.17) to give

$$\frac{\partial u}{\partial r} = \frac{1-N}{2-N}\frac{\partial p}{\partial x}\left\{r - \frac{N(e^{bx} - \phi e^{\omega x}\cos^2\pi(x-t))}{2}\frac{I_1(mr)}{I_1\left(m(e^{bx} - \phi e^{\omega x}\cos^2\pi(x-t))\right)}\right\}, \tag{6.21}$$

Equation (6.19), under the regularity condition, the second one in (6.17), and using equation (6.21), yields

$$w = \frac{1-N}{2(2-N)}\frac{\partial p}{\partial x}\left\{\frac{(e^{bx} - \phi e^{\omega x}\cos^2\pi(x-t))I_1(mr)}{I_1\left(m(e^{bx} - \phi e^{\omega x}\cos^2\pi(x-t))\right)} - r\right\}, \tag{6.22}$$

Further integrating equation (6.22) and using the no-slip condition, first one in (6.17), the axial velocity is derived as

$$u = \frac{1-N}{2(2-N)}\frac{\partial p}{\partial x}\left\{r^2 - \phi^2 e^{2\omega x}\cos^4\pi(x-t) + 2\phi e^{(b+\omega)x}\cos^2\pi(x-t) - e^{2bx}\right.$$
$$\left. + \frac{N(e^{bx} - \phi e^{\omega x}\cos^2\pi(x-t))}{m} \times \left(\frac{I_0\left(m(e^{bx} - \phi e^{\omega x}\cos^2\pi(x-t))\right) - I_0(mr)}{I_1\left(m(e^{bx} - \phi e^{\omega x}\cos^2\pi(x-t))\right)}\right)\right\}. \tag{6.23}$$

where I_0, I_1 are the modified Bessel functions of the 1^{st} kind and the 0^{th} order.

Radial velocity is derived from equation (6.12), using equation (6.23) and integrating it once with respect to r. The regularity condition, given in equation (6.17), is used to get the radial velocity as

$$v = \frac{1-N}{2(2-N)}\Bigg[\Big\{be^{bx} + \frac{\phi e^{\omega x}}{2}(2\pi \sin 2\pi(x-t) - \omega\cos 2\pi(x-t) - \omega)\Big\}\frac{\partial p}{\partial x}$$
$$\Big\{r(e^{bx} - \phi e^{\omega x}\cos^2\pi(x-t)) - \frac{N}{m}\Big\{\frac{r}{2}$$
$$\frac{\partial}{\partial x}\Big(\frac{(e^{bx} - \phi e^{\omega x}\cos^2\pi(x-t))I_0(m(e^{bx} - \phi e^{\omega x}\cos^2\pi(x-t)))}{I_1(m(e^{bx} - \phi e^{\omega x}\cos^2\pi(x-t)))}\Big) - \frac{I_1(mr)}{m}$$
$$\frac{\partial}{\partial x}\Big(\frac{(e^{bx} - \phi e^{\omega x}\cos^2\pi(x-t))}{I_1(m(e^{bx} - \phi e^{\omega x}\cos^2\pi(x-t)))}\Big)\Big\}\Big\} - \frac{\partial^2 p}{\partial x^2}\Big\{\frac{r^3}{4} - \frac{r}{2}(e^{2bx}$$
$$- 2\phi e^{(b+\omega)x}\cos^2\pi(x-t) + \phi^2 e^{2\omega x}\cos^4\pi(x-t))$$
$$+ \frac{N(e^{bx} - \phi e^{\omega x}\cos^2\pi(x-t))}{mI_1(m(e^{bx} - \phi e^{\omega x}\cos^2\pi(x-t)))}\Big(\frac{r}{2}I_0(m(e^{bx} - \phi e^{\omega x}\cos^2\pi(x-t)))$$
$$- \frac{I_1(m(e^{bx} - \phi e^{\omega x}\cos^2\pi(x-t)))}{m}\Big)\Big\}\Bigg]. \quad (6.24)$$

The radial velocity of the fluid at the wall is constrained by the transverse displacement caused by peristaltic waves. Employing this constraint, that is, fourth one in equation (6.17), on the radial velocity in terms of the wall displacement given in equation (6.16), we get the expression

$$
\begin{aligned}
-\frac{\pi\phi}{4}e^{\omega x}\Big[\Big(2\phi e^{\omega x}-4e^{bx}\Big)\sin 2\pi(x-t)\ +\phi e^{\omega x}\sin 4\pi(x-t)\ \Big] &= \frac{1-N}{2(2-N)}\Bigg[\Bigg\{be^{bx}\\
&+\frac{\phi e^{\omega x}}{2}\Big(2\pi\sin 2\pi(x-t)\ -\omega\cos 2\pi(x-t)-\omega\ \Big)\Bigg\}\\
\frac{\partial p}{\partial x}\Bigg\{e^{3bx}-\phi^3 e^{3\omega x}\cos^6\pi(x-t)-3\phi e^{(2b+\omega)x}\cos^2\pi(x-t)+3\phi^2 e^{(b+2\omega)x}\cos^4\pi(x-t)&\\
-\frac{Ne^{bx}-\phi e^{\omega x}\cos^2\pi(x-t)}{m}\times\Bigg\{\frac{(e^{bx}-\phi e^{\omega x}\cos^2\pi(x-t))}{2}\frac{\partial}{\partial x}&\\
\left(\frac{(e^{bx}-\phi e^{\omega x}\cos^2\pi(x-t))I_0\Big(m(e^{bx}-\phi e^{\omega x}\cos^2\pi(x-t))\Big)}{I_1\Big(m(e^{bx}-\phi e^{\omega x}\cos^2\pi(x-t))\Big)}\right)&\\
-\frac{I_1\Big(m(e^{bx}-\phi e^{\omega x}\cos^2\pi(x-t))\Big)}{m}\frac{\partial}{\partial x}\left(\frac{(e^{bx}-\phi e^{\omega x}\cos^2\pi(x-t))}{I_1\Big(m(e^{bx}-\phi e^{\omega x}\cos^2\pi(x-t))\Big)}\right)\Bigg\}\Bigg\}&\\
+\frac{\partial^2 p}{\partial x^2}\Bigg\{-\phi e^{(3b+\omega)x}\cos^2\pi(x-t)\ -\phi^3 e^{(b+3\omega)x}\cos^6\pi(x-t)&\\
+\frac{e^{4bx}+\phi^4 e^{4\omega x}\cos^8\pi(x-t)+6\phi^2 e^{2(b+\omega)x}\cos^4\pi(x-t)}{4}&\\
+\frac{N(e^{bx}-\phi e^{\omega x}\cos^2\pi(x-t))^2}{2m^2}&\\
\left(2-\frac{m(e^{bx}-\phi e^{\omega x}\cos^2\pi(x-t))I_0\Big(m(e^{bx}-\phi e^{\omega x}\cos^2\pi(x-t))\Big)}{I_1\Big(m(e^{bx}-\phi e^{\omega x}\cos^2\pi(x-t))\Big)}\right)\Bigg\}\Bigg]. &\qquad (6.25)
\end{aligned}
$$

The pressure gradient is obtained in an explicit form by the integration of equation (6.25) with respect to x, followed by some manipulation on the two sides. This gives

$$\frac{1-N}{8(2-N)}\frac{\partial p}{\partial x}=$$
$$\frac{S(t)+\frac{\pi\phi}{4}\int_0^x e^{\omega x}\left[\left(2\phi e^{\omega x}-4e^{bx}\right)\sin 2\pi(x-t)\ +\phi e^{\omega x}\sin 4\pi(x-t)\ \right]ds}{\phi^4 e^{4\omega x}\cos^8\pi(x-t)+6\phi^2 e^{2(b+\omega)x}\cos^4\pi(x-t)-4\phi e^{(3b+\omega)x}\cos^2\pi(x-t)} \tag{6.26}$$
$$-4\phi^3 e^{(b+3\omega)x}\cos^6\pi(x-t)+e^{4bx}$$
$$+\frac{4N(e^{bx}-\phi e^{\omega x}\cos^2\pi(x-t))^2}{m^2}\left(1-\frac{m(e^{bx}-\phi e^{\omega x}\cos^2\pi(x-t))I_0\left(m(e^{bx}-\phi e^{\omega x}\cos^2\pi(x-t))\right)}{2I_1\left(m(e^{bx}-\phi e^{\omega x}\cos^2\pi(x-t))\right)}\right)$$

where $S(t)$ is a function of t to be evaluated later.

If we integrating equation (6.26) once again from 0 to x we get the useful expression for pressure difference as

$$(p(x,\ t)-p(0,\ t))\times\left\{\frac{1-N}{8(2-N)}\right\}=$$
$$\int_0^x \frac{S(t)+\frac{\pi\phi}{4}\int_0^s e^{\omega x}\left[\left(2\phi e^{\omega x}-4e^{bx}\right)\sin 2\pi(x-t)\ +\phi e^{\omega x}\sin 4\pi(x-t)\ \right]ds_1}{\phi^4 e^{4\omega x}\cos^8\pi(x-t)+6\phi^2 e^{2(b+\omega)x}\cos^4\pi(x-t)-4\phi e^{(3b+\omega)x}\cos^2\pi(x-t)}ds,$$
$$-4\phi^3 e^{(b+3\omega)x}\cos^6\pi(x-t)$$
$$+e^{4bx}+\frac{4N(e^{bx}-\phi e^{\omega x}\cos^2\pi(x-t))^2}{m^2}\left(1-\frac{m(e^{bx}-\phi e^{\omega x}\cos^2\pi(x-t))I_0\left(m(e^{bx}-\phi e^{\omega x}\cos^2\pi(x-t))\right)}{2I_1\left(m(e^{bx}-\phi e^{\omega x}\cos^2\pi(x-t))\right)}\right) \tag{6.27}$$

The pressure difference between the inlet and the outlet of the tube is readily obtained by substituting $x=l$ in equation (6.27), which is

$$(p(l,\ t)-p(0,\ t))\times\left\{\frac{1-N}{8(2-N)}\right\}=$$
$$\int_0^l \frac{S(t)+\frac{\pi\phi}{4}\int_0^x e^{\omega x}\left[\left(2\phi e^{\omega x}-4e^{bx}\right)\sin 2\pi(x-t)\ +\phi e^{\omega x}\sin 4\pi(x-t)\ \right]ds}{\phi^4 e^{4\omega x}\cos^8\pi(x-t)+\ 6\phi^2 e^{2(b+\omega)x}\cos^4\pi(x-t)-4\phi e^{(3b+\omega)x}\cos^2\pi(x-t)} dx,$$
$$-4\phi^3 e^{(b+3\omega)x}\cos^6\pi(x-t)$$
$$+e^{4bx}+\frac{4N(e^{bx}-\phi e^{\omega x}\cos^2\pi(x-t))^2}{m^2}\left(1-\frac{m(e^{bx}-\phi e^{\omega x}\cos^2\pi(x-t))I_0\left(m(e^{bx}-\phi e^{\omega x}\cos^2\pi(x-t))\right)}{2I_1\left(m(e^{bx}-\phi e^{\omega x}\cos^2\pi(x-t))\right)}\right) \tag{6.28}$$

$S(t)$ may be evaluated by a simple manipulation of equation (6.28), as

$$S(t)=$$
$$\frac{\frac{1-N}{8(2-N)}\Delta p_l(t)}{-\int_0^l \frac{\frac{\pi\phi}{4}\int_0^x e^{\omega x}\left[\left(2\phi e^{\omega x}-4e^{bx}\right)\sin 2\pi(x-t)\ +\phi e^{\omega x}\sin 4\pi(x-t)\ \right]ds}{\phi^4 e^{4\omega x}\cos^8\pi(x-t)+\ 6\phi^2 e^{2(b+\omega)x}\cos^4\pi(x-t)-4\phi e^{(3b+\omega)x}\cos^2\pi(x-t)} dx}$$
$$-4\phi^3 e^{(b+3\omega)x}\cos^6\pi(x-t)$$
$$+e^{4bx}+\frac{4N(e^{bx}-\phi e^{\omega x}\cos^2\pi(x-t))^2}{m^2}\left(1-\frac{m(e^{bx}-\phi e^{\omega x}\cos^2\pi(x-t))I_0\left(m(e^{bx}-\phi e^{\omega x}\cos^2\pi(x-t))\right)}{2I_1\left(m(e^{bx}-\phi e^{\omega x}\cos^2\pi(x-t))\right)}\right)$$
$$\int_0^l \frac{1}{\phi^4 e^{4\omega x}\cos^8\pi(x-t)+\ 6\phi^2 e^{2(b+\omega)x}\cos^4\pi(x-t)-4\phi e^{(3b+\omega)x}\cos^2\pi(x-t)} dx,$$
$$-4\phi^3 e^{(b+3\omega)x}\cos^6\pi(x-t)$$
$$+e^{4bx}+\frac{4N(e^{bx}-\phi e^{\omega x}\cos^2\pi(x-t))^2}{m^2}\left(1-\frac{m(e^{bx}-\phi e^{\omega x}\cos^2\pi(x-t))I_0\left(m(e^{bx}-\phi e^{\omega x}\cos^2\pi(x-t))\right)}{2I_1\left(m(e^{bx}-\phi e^{\omega x}\cos^2\pi(x-t))\right)}\right) \tag{6.29}$$

where $\Delta p_l(t)=p(l,\ t)-p(0,\ t)$, denotes the difference between the pressures at the inlet and the outlet.

6.3.1 Time averaged volume flow rate

The volume flow rate for single wave propagation is defined as

$$Q(x,\ t) = \int_0^h 2rudr,$$

Performing integration we get

$$\begin{aligned} Q(x,\ t) = \frac{N-1}{4(2-N)}\frac{\partial p}{\partial x}\{&\phi^4 e^{4\omega x}\cos^8\pi(x-t) + 6\phi^2 e^{2(b+\omega)x}\cos^4\pi(x-t) \\ &- 4\phi^3 e^{(b+3\omega)x}\cos^6\pi(x-t) \\ &- 4\phi e^{(3b+\omega)x}\cos^2\pi(x-t) + e^{4bx} + \frac{4N(e^{bx}-\phi e^{\omega x}\cos^2\pi(x-t))^2}{m^2} \\ &\left(1 - \frac{m(e^{bx}-\phi e^{\omega x}\cos^2\pi(x-t))I_0\left(m(e^{bx}-\phi e^{\omega x}\cos^2\pi(x-t))\right)}{2I_1\left(m(e^{bx}-\phi e^{\omega x}\cos^2\pi(x-t))\right)}\right)\}, \end{aligned} \tag{6.30}$$

Time-averaged volume flow rate will be

$$\begin{aligned} \tilde{Q} = \frac{N-1}{4(2-N)}\int_0^1 \frac{\partial p}{\partial x}\{&\phi^4 e^{4\omega x}\cos^8\pi(x-t) + 6\phi^2 e^{2(b+\omega)x}\cos^4\pi(x-t) \\ &- 4\phi^3 e^{(b+3\omega)x}\cos^6\pi(x-t) \\ &- 4\phi e^{(3b+\omega)x}\cos^2\pi(x-t) + e^{4bx} + \frac{4N(e^{bx}-\phi e^{\omega x}\cos^2\pi(x-t))^2}{m^2} \\ &\left(1 - \frac{m(e^{bx}-\phi e^{\omega x}\cos^2\pi(x-t))I_0\left(m(e^{bx}-\phi e^{\omega x}\cos^2\pi(x-t))\right)}{2I_1\left(m(e^{bx}-\phi e^{\omega x}\cos^2\pi(x-t))\right)}\right)\}dt \end{aligned} \tag{6.31}$$

Wave frame and laboratory frame relation for time-averaged volume flow rate is:

$$\tilde{Q} = q + e^{2bx} - \phi e^{(b+\omega)x} + \frac{3}{8}\phi^2 e^{2\omega x},$$

$$= Q + \phi e^{(b+\omega)x}\cos 2\pi(x-t) - \frac{1}{8}(\cos 4\pi(x-t) + 4\cos 2\pi(x-t))\phi^2 e^{2\omega x}, \quad (6.32)$$

Thus the pressure gradient in terms of the time-averaged volume flow rate may be given with some manipulations of equations (6.30) and (6.32), by

$$\frac{\partial p}{\partial x} \times \left\{\frac{N-1}{4(2-N)}\right\} =$$

$$\left\{\begin{array}{c} \\ \\ \\ \dfrac{\tilde{Q} - \phi e^{(b+\omega)x}\cos 2\pi(x-t) + \frac{1}{8}(\cos 4\pi(x-t) + 4\cos 2\pi(x-t))\phi^2 e^{2\omega x}}{\phi^4 e^{4\omega x}\cos^8\pi(x-t) + 6\phi^2 e^{2(b+\omega)x}\cos^4\pi(x-t) - 4\phi e^{(3b+\omega)x}\cos^2\pi(x-t)} \\ -4\phi^3 e^{(b+3\omega)x}\cos^6\pi(x-t) \\ +e^{4bx} + \frac{4N(e^{bx}-\phi e^{\omega x}\cos^2\pi(x-t))^2}{m^2}\left(1 - \frac{m(e^{bx}-\phi e^{\omega x}\cos^2\pi(x-t))I_0\left(m(e^{bx}-\phi e^{\omega x}\cos^2\pi(x-t))\right)}{2I_1\left(m(e^{bx}-\phi e^{\omega x}\cos^2\pi(x-t))\right)}\right) \\ \\ \\ \end{array}\right\},$$

(6.33)

In terms of the time-averaged volume flow rate, the pressure gradient is given by

$$(p(x)-p(0))\times\left\{\frac{N-1}{4(2-N)}\right\}=$$
$$\int_0^x \frac{\tilde{Q}-\phi e^{(b+\omega)x}\cos 2\pi(x-t)\ +\frac{1}{8}(\cos 4\pi(x-t)+4\cos 2\pi(x-t)\ )\phi^2 e^{2\omega x}}{\phi^4 e^{4\omega x}\cos^8\pi(x-t)+6\phi^2 e^{2(b+\omega)x}\cos^4\pi(x-t)-4\phi e^{(3b+\omega)x}\cos^2\pi(x-t)} ds,$$
$$-4\phi^3 e^{(b+3\omega)x}\cos^6\pi(x-t)$$
$$+e^{4bx}+\frac{4N(e^{bx}-\phi e^{\omega x}\cos^2\pi(x-t))^2}{m^2}\left(1-\frac{m(e^{bx}-\phi e^{\omega x}\cos^2\pi(x-t))I_0\left(m(e^{bx}-\phi e^{\omega x}\cos^2\pi(x-t))\right)}{2I_1\left(m(e^{bx}-\phi e^{\omega x}\cos^2\pi(x-t))\right)}\right) \tag{6.34}$$

which, for $x=l$, is

$$(p(l)-p(0))\times\left\{\frac{N-1}{4(2-N)}\right\}=$$
$$\int_0^l \frac{\tilde{Q}-\phi e^{(b+\omega)x}\cos 2\pi(x-t)\ +\frac{1}{8}(\cos 4\pi(x-t)+4\cos 2\pi(x-t)\ )\phi^2 e^{2\omega x}}{\phi^4 e^{4\omega x}\cos^8\pi(x-t)+6\phi^2 e^{2(b+\omega)x}\cos^4\pi(x-t)-4\phi e^{(3b+\omega)x}\cos^2\pi(x-t)} dx,$$
$$-4\phi^3 e^{(b+3\omega)x}\cos^6\pi(x-t)$$
$$+e^{4bx}+\frac{4N(e^{bx}-\phi e^{\omega x}\cos^2\pi(x-t))^2}{m^2}\left(1-\frac{m(e^{bx}-\phi e^{\omega x}\cos^2\pi(x-t))I_0\left(m(e^{bx}-\phi e^{\omega x}\cos^2\pi(x-t))\right)}{2I_1\left(m(e^{bx}-\phi e^{\omega x}\cos^2\pi(x-t))\right)}\right) \tag{6.35}$$

Finally, the local wall shear stress is defined as

$$\tau_w=\left.\frac{\partial u}{\partial r}\right|_{r=h},$$

which by equation (6.21) is of the form

$$\tau_w = \frac{(1-N)\,h}{2}\frac{\partial p}{\partial x},$$

and reduces, due to equation (6.26), to

$$\frac{\tau_w}{4(2-N)} = \left[\frac{S(t)+\frac{\pi\phi}{4}\int_0^x e^{\omega x}[\left(2\phi e^{\omega x}-4e^{bx}\right)\sin 2\pi(x-t)+\phi e^{\omega x}\sin 4\pi(x-t)\,]ds}{e^{3bx}-\phi^3 e^{3\omega x}\cos^6\pi(x-t)\;-3\phi e^{(2b+\omega)x}\cos^2\pi(x-t)\;+3\phi^2 e^{(b+2\omega)x}\cos^4\pi(x-t)\;+\frac{4N(e^{bx}-\phi e^{\omega x}\cos^2\pi(x-t))}{m^2}\left(1-\frac{m(e^{bx}-\phi e^{\omega x}\cos^2\pi(x-t))I_0\left(m(e^{bx}-\phi e^{\omega x}\cos^2\pi(x-t))\right)}{2I_1\left(m(e^{bx}-\phi e^{\omega x}\cos^2\pi(x-t))\right)}\right)}\right], \tag{6.36}$$

6.3.2 Reflux limit

Reflux refers to the presence of fluid particles that move, on the average, in a direction opposite to the net flow in the close vicinity of the wall (Shapiro *et al.* (1969)). The dimensional form of stream function in the wave frame is given by

$$d\widetilde{\psi} = 2\pi\tilde{R}\left(\tilde{U}d\tilde{R}-\tilde{V}d\tilde{X}\right), \tag{6.37}$$

for the axi-symmetric flow, where $\widetilde{\psi}$, $\tilde{X},\tilde{R}$, $\tilde{U}$ and $\tilde{V}$ are stream function, axial coordinates, velocities components respectively.

We use the transformations between the wave and the laboratory frames, defined as

$$\tilde{X} = \tilde{x} - c\tilde{t},\ \tilde{R} = \tilde{r},\ \tilde{U} = \tilde{u} - c,\ \tilde{V} = \tilde{v},\ \tilde{q} = \tilde{Q} - c\tilde{h}^2,\ \widetilde{\Psi} = \widetilde{\psi} - \tilde{r}^2, \tag{6.38}$$

where the left side of the parameters is in the wave frame while the right side of the parameters are in the laboratory frame, we obtain stream function as

$$\psi = -\left[r^2 + \frac{num}{denom}\right], \tag{6.39}$$

where

$$num = \begin{array}{c} \left(\tilde{Q} - \phi e^{(b+\omega)x}\cos 2\pi(x-t) + \frac{1}{8}\left(\cos 4\pi(x-t)\right.\right. \\ \left.\left. +4\cos 2\pi(x-t)\right)\phi^2 e^{2\omega x}\right)\times \\ \left\{r^4 - 2r^2(e^{bx} - \phi e^{\omega x}\cos^2\pi(x-t))^2\right. \\ \left. + \frac{2N(e^{bx}-\phi e^{\omega x}\cos^2\pi(x-t))\left(mI_0\left(m(e^{bx}-\phi e^{\omega x}\cos^2\pi(x-t))\right)r^2 - 2rI_1(mr)\right)}{m^2 I_1\left(m(e^{bx}-\phi e^{\omega x}\cos^2\pi(x-t))\right)}\right\} \end{array}$$

$$denom = \begin{array}{c} \phi^4 e^{4\omega x}\cos^8\pi(x-t) + 6\phi^2 e^{2(b+\omega)x}\cos^4\pi(x-t) - 4\phi e^{(3b+\omega)x}\cos^2\pi(x-t) \\ -4\phi^3 e^{(b+3\omega)x}\cos^6\pi(x-t) \\ +e^{4bx} + \frac{4N(e^{bx}-\phi e^{\omega x}\cos^2\pi(x-t))^2}{m^2} \\ \left(1 - \frac{m(e^{bx}-\phi e^{\omega x}\cos^2\pi(x-t))I_0\left(m(e^{bx}-\phi e^{\omega x}\cos^2\pi(x-t))\right)}{2I_1\left(m(e^{bx}-\phi e^{\omega x}\cos^2\pi(x-t))\right)}\right) \end{array}$$

Stream function at the wall, ψ_w is solved from equation (6.39) by putting $r = h$. Simplification gives

$$\psi|_{r=h}= \psi_w = \tilde{Q} - e^{2bx} + \phi e^{(b+\omega)x} - \frac{3}{8}\phi^2 e^{2\omega x}, \tag{6.40}$$

Reflux flow rate, $Q_\psi(x)$ associated with a particle at the position x is given by

$$Q_\psi(x) = \psi + r^2(\psi,\ x), \tag{6.41}$$

which, on averaging over one cycle, gives

$$\tilde{Q}_\psi = \psi + \int_0^1 r^2(\psi,\ x)dx, \tag{6.42}$$

Further, $\tilde{Q}_\psi$ is expressed in a power series, in terms of a small parameter ε about the wall to determine the reflux limit, where $\varepsilon\left(=\psi-\psi_w\right)$ is subjected to the reflux condition

$$\frac{\tilde{Q}_\psi}{\tilde{Q}} > 1 \text{ as } \varepsilon \to 0, \tag{6.43}$$

The coefficient of the first two terms in the expansion of r are obtained only for small values of m. Substituting the expansion $r^2(\psi,x) = h^2 + a_1\varepsilon + a_2\varepsilon^2 + a_3\varepsilon^3 + \ldots$ into equations (6.39), and using equations (6.40), we get

$$a_1 = -1, \tag{6.44}$$

$$a_2 = -\left[\frac{\left(1-\frac{1}{4}\frac{mN(e^{bx}-\phi e^{\omega x}\cos^2\pi(x-t))}{I_1\left(m(e^{bx}-\phi e^{\omega x}\cos^2\pi(x-t))\right)}\right)\left(\tilde{Q}-\phi e^{(b+\omega)x}\cos 2\pi(x-t)+\frac{1}{8}\left(\cos 4\pi(x-t)+4\cos 2\pi(x-t)\right)\phi^2 e^{2\omega x}\right)}{\phi^4 e^{4\omega x}\cos^8\pi(x-t)+6\phi^2 e^{2(b+\omega)x}\cos^4\pi(x-t)-4\phi e^{(3b+\omega)x}\cos^2\pi(x-t)-4\phi^3 e^{(b+3\omega)x}\cos^6\pi(x-t)+e^{4bx}+\frac{4N(e^{bx}-\phi e^{\omega x}\cos^2\pi(x-t))^2}{m^2}\left(1-\frac{m(e^{bx}-\phi e^{\omega x}\cos^2\pi(x-t))I_0\left(m(e^{bx}-\phi e^{\omega x}\cos^2\pi(x-t))\right)}{2I_1\left(m(e^{bx}-\phi e^{\omega x}\cos^2\pi(x-t))\right)}\right)}\right], \tag{6.45}$$

Integrating equation (6.41) with respect to x by using equations (6.42)-(6.45), we obtain the reflux limit as

$$\tilde{Q} < e^{2bx}-\phi e^{(b+\omega)x}+\frac{3}{8}\phi^2 e^{2\omega x} - \frac{\int_0^1 \frac{\left(1-\frac{1}{4}\frac{mN(e^{bx}-\phi e^{\omega x}\cos^2\pi(x-t))}{I_1\left(m(e^{bx}-\phi e^{\omega x}\cos^2\pi(x-t))\right)}\right)}{e^{2bx}+\phi^2 e^{2\omega x}\cos^4\pi(x-t)-2\phi e^{(b+\omega)x}\cos^2\pi(x-t)+\frac{4N}{m^2}\left(1-\frac{m(e^{bx}-\phi e^{\omega x}\cos^2\pi(x-t))I_0\left(m(e^{bx}-\phi e^{\omega x}\cos^2\pi(x-t))\right)}{2I_1\left(m(e^{bx}-\phi e^{\omega x}\cos^2\pi(x-t))\right)}\right)}dx}{\int_0^1 \frac{\left(1-\frac{1}{4}\frac{mN(e^{bx}-\phi e^{\omega x}\cos^2\pi(x-t))}{I_1\left(m(e^{bx}-\phi e^{\omega x}\cos^2\pi(x-t))\right)}\right)}{\phi^4 e^{4\omega x}\cos^8\pi(x-t)+6\phi^2 e^{2(b+\omega)x}\cos^4\pi(x-t)-4\phi e^{(3b+\omega)x}\cos^2\pi(x-t)-4\phi^3 e^{(b+3\omega)x}\cos^6\pi(x-t)+e^{4bx}+\frac{4N(e^{bx}-\phi e^{\omega x}\cos^2\pi(x-t))^2}{m^2}\left(1-\frac{m(e^{bx}-\phi e^{\omega x}\cos^2\pi(x-t))I_0\left(m(e^{bx}-\phi e^{\omega x}\cos^2\pi(x-t))\right)}{2I_1\left(m(e^{bx}-\phi e^{\omega x}\cos^2\pi(x-t))\right)}\right)}dx}, \tag{6.46}$$

6.4 Numerical results and discussion

The intention behind this investigation is to comprehend the impact of moderate abdominal protrusion above cardiac sphincter, clinically called sliding hiatus hernia, on swallowing of micro-polar fluid with dilating peristaltic waves. We classify the cross-sectional deformation of the tube into two types for investigation:

Case 1: The tube diverges from the beginning through the end. The divergence is although mild but fits an exponential curve.

Case 2: The tube diverges only near the distal end but still is of the exponential nature so that it models the reality.

We assume a single bolus of micropolar fluid to swallow in the tube which is thrice its size. This is because, in practice, only one bolus moves in the oesophagus when fluid is not Newtonian. We further consider the two ends of the tube at zero pressure to consider contribution of merely propagating peristaltic waves.

The parameters in this problem that mainly impact the flow are the dilation parameter ω which increases the wave amplitude, the gradient parameter b which changes the cross-sectional area of the tube, the coupling number $N\,(0 \leq N \leq 1)$ which is a measure of particle coupling with its surroundings and the micro-polar parameter m.

6.4.1 Divergence along the entire length of the tube

In this section, we shall discuss temporal and spatial pressure distribution by computer simulation.

6.4.1.1 Effect of wave amplitude dilation

Pressure distribution is plotted for $t = 0.0, 0.25, 0.50, 0.75, 1.0, 1.25, 1.50, 1.75$. Since the bolus is considered already inside the tube, there is no further scope for the bolus to travel inside the tube. The effect of dilation of wave amplitude ω on the flow dynamics is plotted in Figure 6.3. The various parameters are set as $l = 3,\ \phi = 0.7,\ N = 0.20,\ b = 0.04,\ m = 1.00$ while t is varied in the range $0 - 2$ for three distinct values of $\omega = 0.0, 0.03, 0.06$. Difference of the maximum and the minimum pressures increases very significantly along the axis with larger ω contributing larger difference, endorsing the experimental report of Kahrilas *et al*. (1999) even when the tube diverges. Thus, the cross-sectional increase does not affect flow adversely.

6.4.1.2 Effect of Coupling Number

The next set of diagrams in Figure 6.4 are meant to examine the influence of the coupling number N which is varied in the range $0.00 - 0.90$ with fixed $\omega = 0.001$. The observation is that pressure increases with N. Thus, we infer that non-Newtonian nature of this kind of fluid requires more pressure.

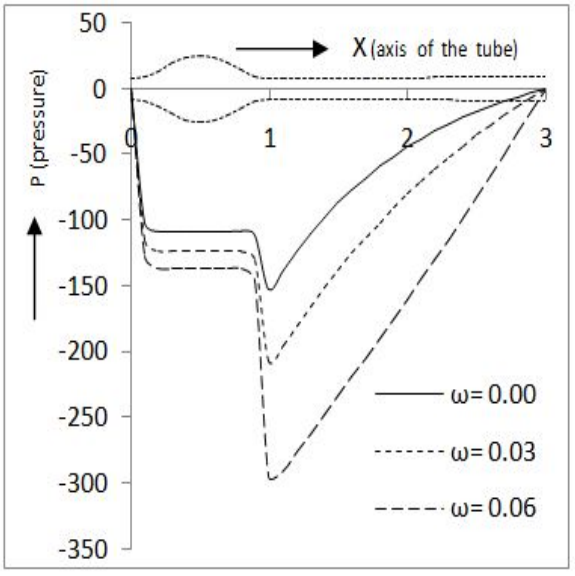

(6.3a) $t = 0.00$

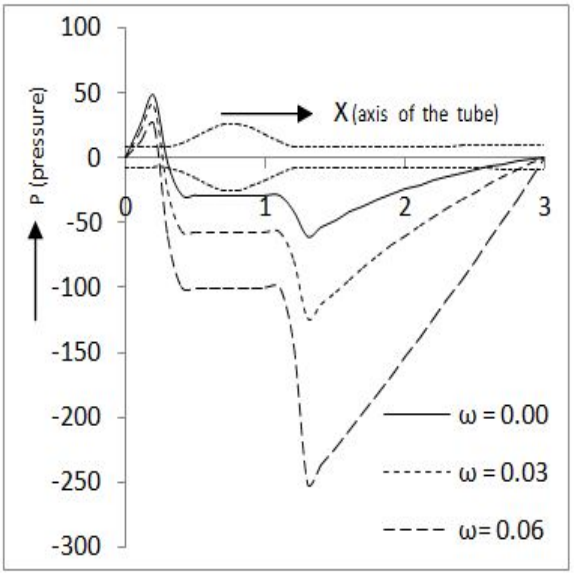

(6.3b) $t = 0.25$

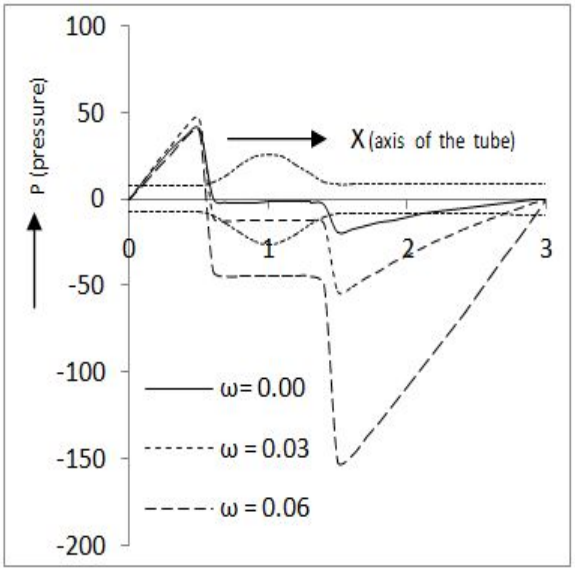

(6.3c) $t = 0.50$

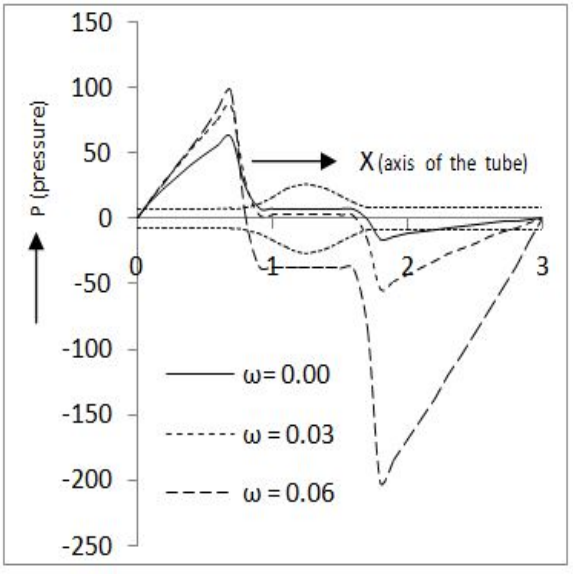

(6.3d) $t = 0.75$

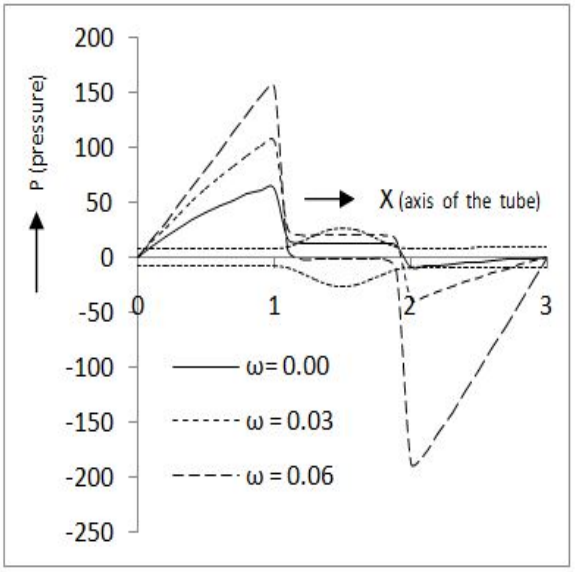

(6.3e) $t = 1.00$

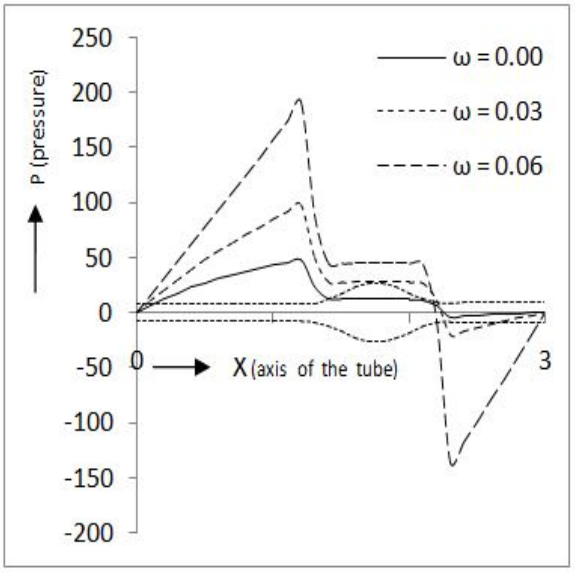

(6.3f) $t = 1.25$

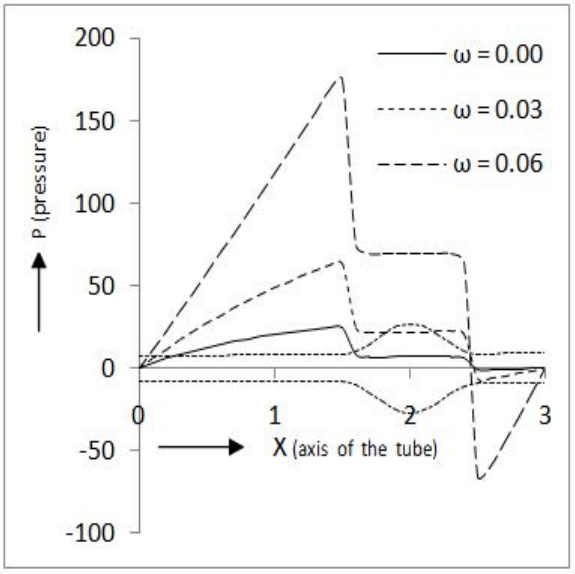

(6.3g) $t = 1.50$

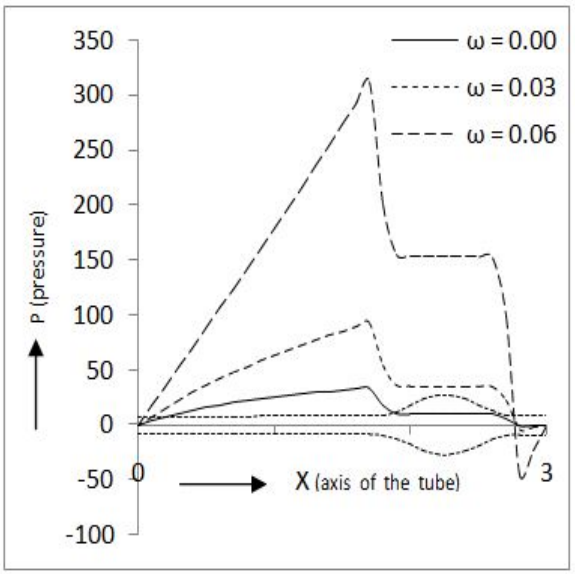

(6.3h) $t = 1.75$

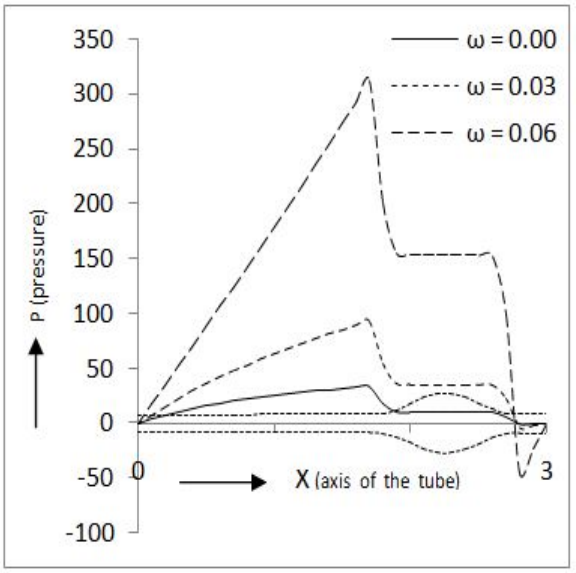

(6.3i) $t = 2.00$

Figure 6.3: Pressure distribution along axial distance at different time instant showing the effect of dilation parameter ω. Other parameters are taken as $l = 3,\ \phi = 0.7,\ N = 0.20,\ b = 0.04,\ m = 1.00$.

6.4.1.3 Effect of micropolar parameter

We further test the impact of the micropolar parameter m which is varied from $2.00 - 6.00$ with fixed $N = 0.20$. Figure 6.5 reveals that the larger the value of the micropolar parameter, the lower is the pressure required for flow.

6.4.1.4 Effect of gradient parameter

The tube is let diverge right from the beginning. Another case, in which tube diverges only near the other end, will be discussed later in section 6.4.2. Positive value assigned to b will increase the cross section exponentially. Linear divergence is a special case. Figure 6.6 contains plots showing the effect of gradient parameter b which makes the tube diverge. This is the main aspect of this investigation. Other parameters are set as $l = 3,\ \phi = 0.7,\ \omega = 0.001,\ N = 0.20,\ m = 1.00$.

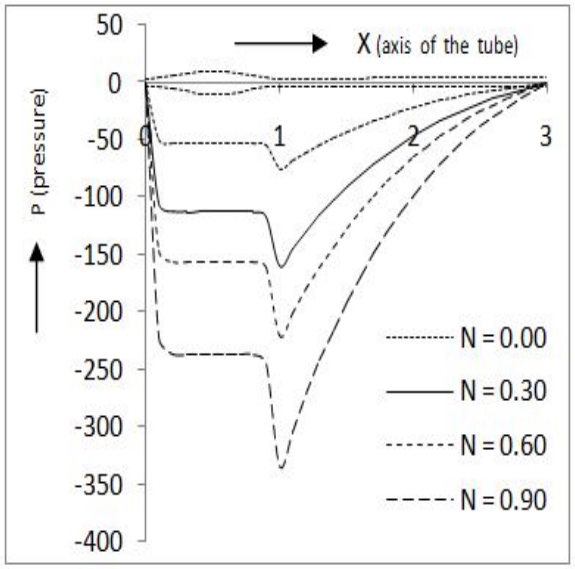

(6.4a) $t = 0.00$

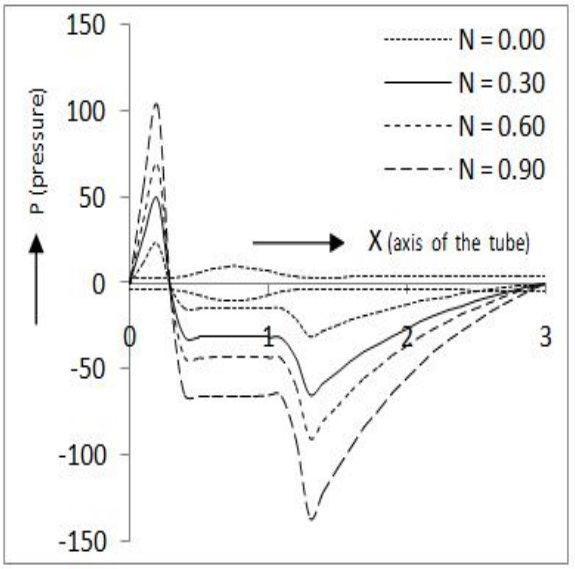

(6.4b) $t = 0.25$

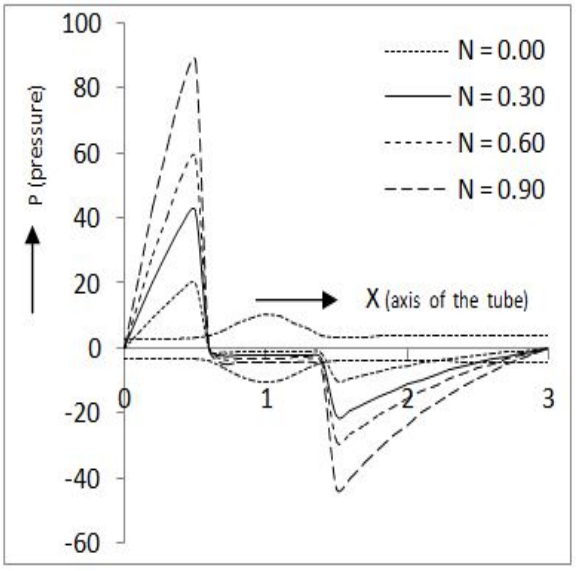

(6.4c) $t = 0.50$

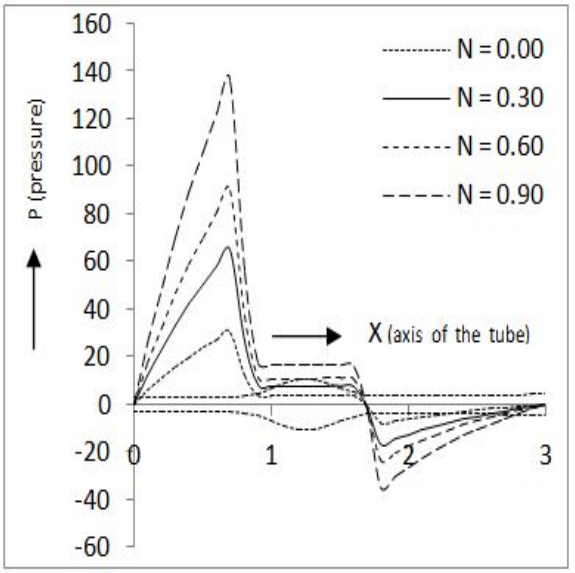

(6.4d) $t = 0.75$

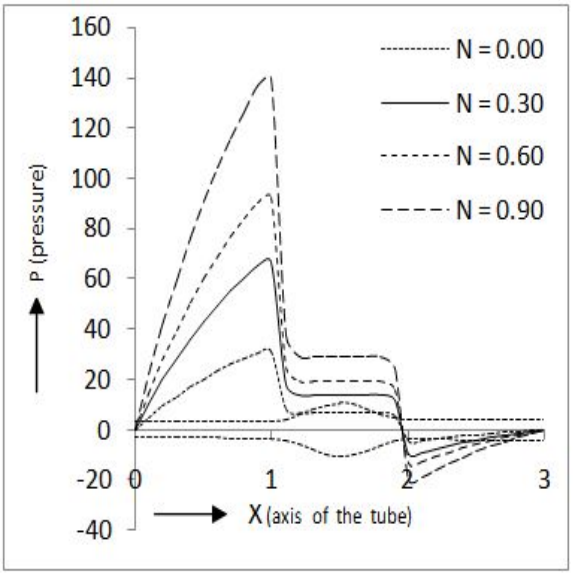

(6.4e) $t = 1.00$

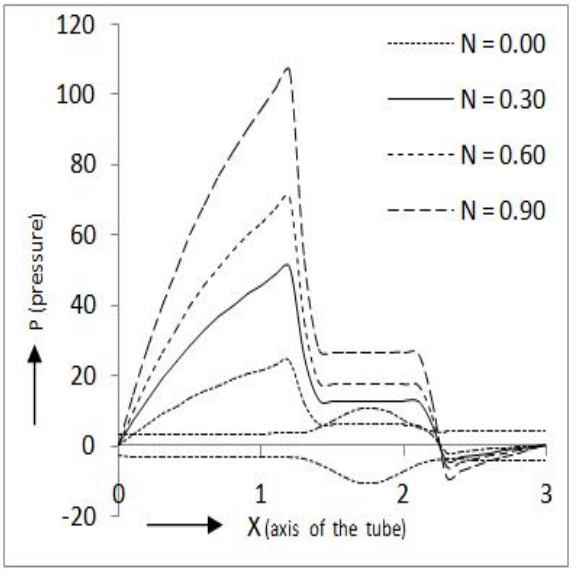

(6.4f) $t = 1.25$

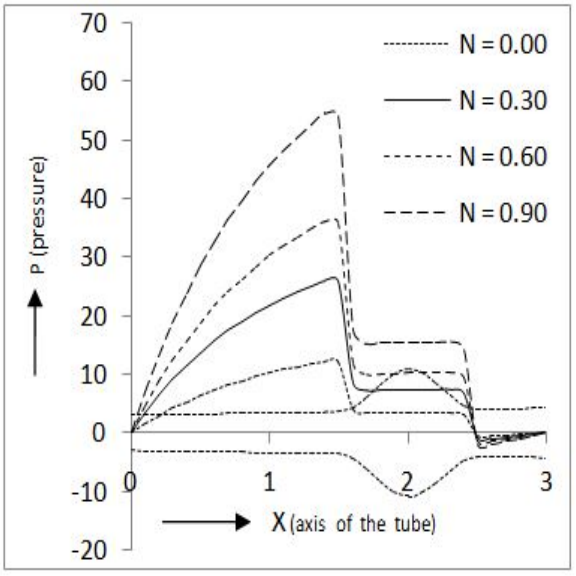

(6.4g) $t = 1.50$

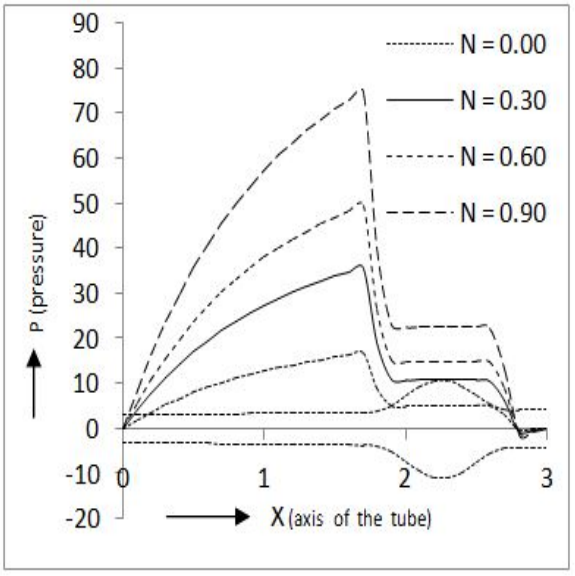

(6.4h) $t = 1.75$

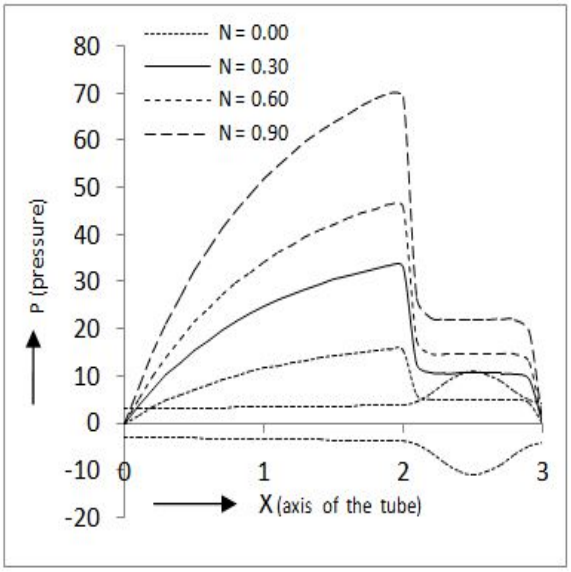

(6.4i) $t = 2.00$

Figure 6.4: Pressure distribution along axial distance at different time instant showing the effect of coupling number N. Other parameters are taken as $l = 3,\ \phi = 0.7,\ \omega = 0.001,\ b = 0.04,\ m = 1.00$.

It is observed in all plots that pressure drops as b increases, which indicates less pressure requirement for flow. The case $b = 0$ used for comparison corresponds to the uniform tube. This also indicates that exponential divergence in the geometrical shape of the tube makes pressure decline more compared to linear divergence (Chandra and Pandey (2018); Pandey and Singh (2019).

6.4.1.5 Effect on wall shear stress

In this section we shall discuss impacts of the wave amplitude dilation and the gradient parameters on wall shear stress.

We fix $l = 3,\ \phi = 0.7,\ N = 0.20,\ b = 0.04,\ m = 1.0$ and let the wave amplitude dilation parameter ω vary from $0.0 - 0.06$. The wave amplitude dilation parameter ω is observed to enhance wall shear stress τ_w all along the tube axis at all temporal values as it increases in magnitude [Figure 6.7].

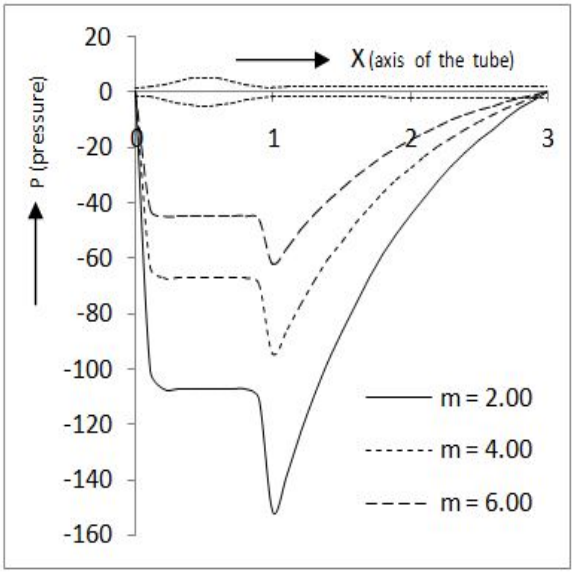

(6.5a) $t = 0.00$

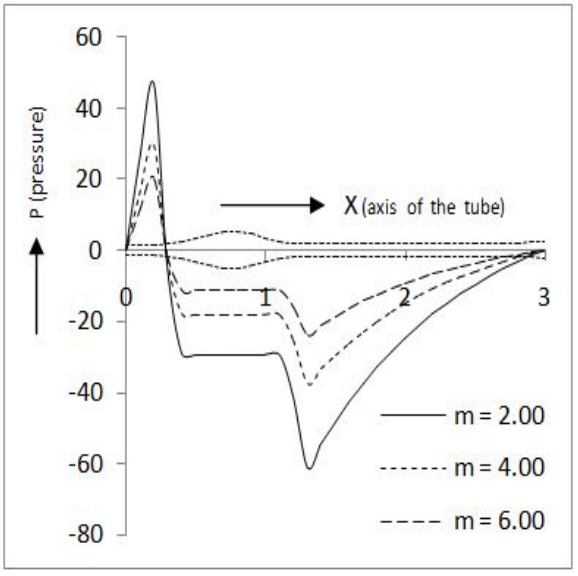

(6.5b) $t = 0.25$

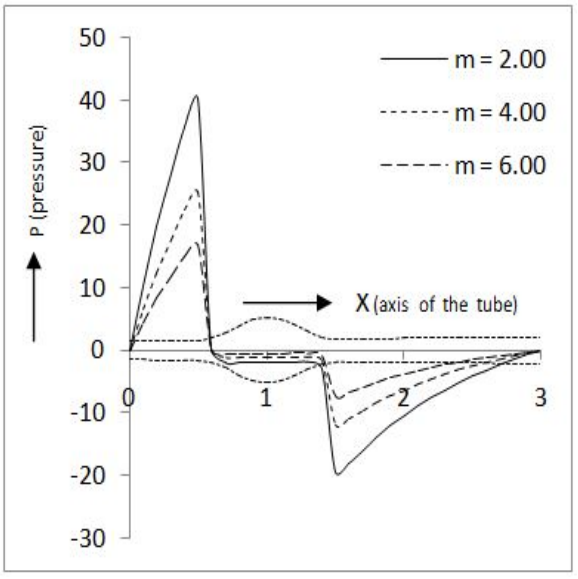

(6.5c) $t = 0.50$

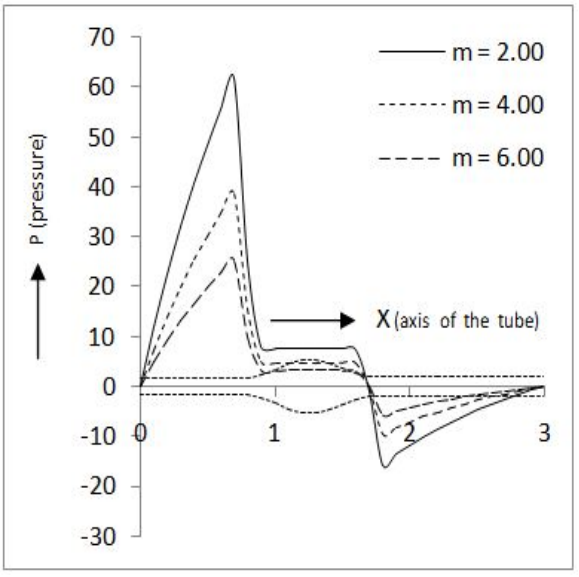

(6.5d) $t = 0.75$

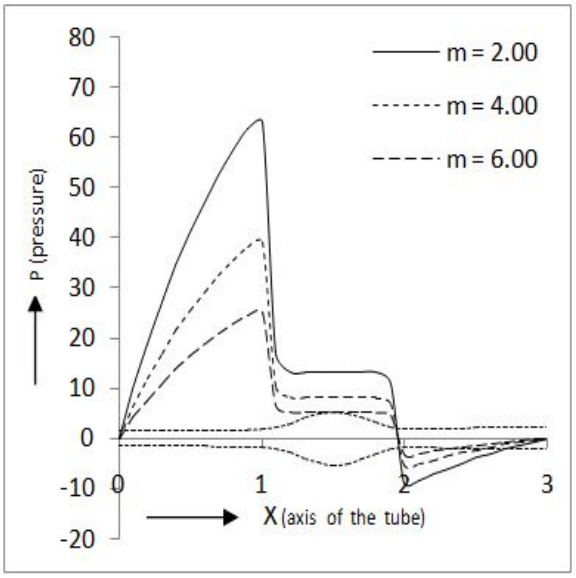

(6.5e) $t = 1.00$

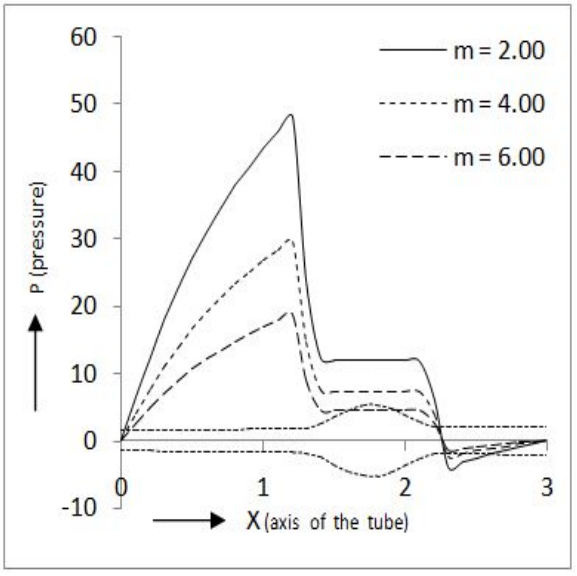

(6.5f) $t = 1.25$

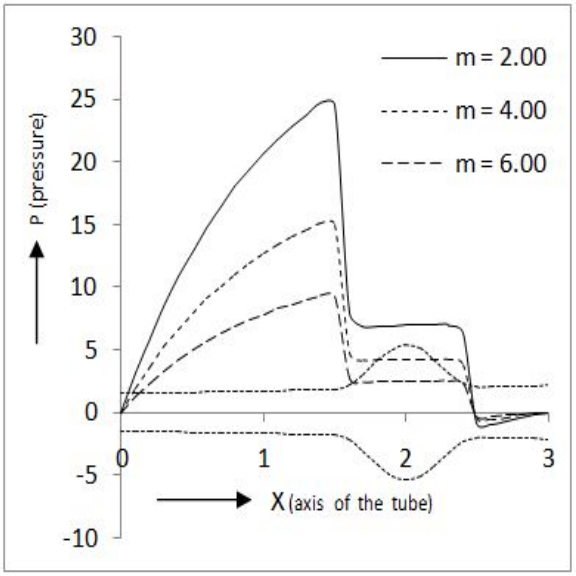

(6.5g) $t = 1.50$

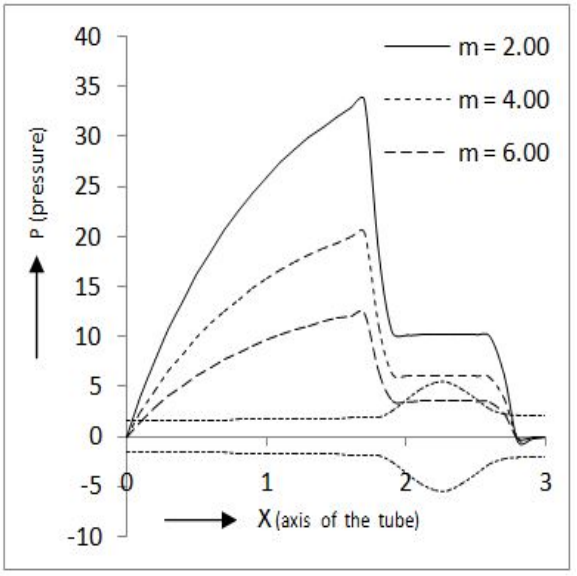

(6.5h) $t = 1.75$

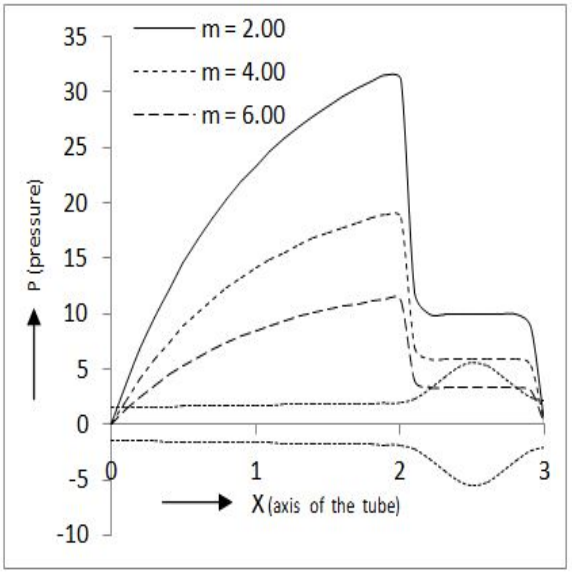

(6.5i) $t = 2.00$

Figure 6.5: Pressure distribution along axial distance at different time instant showing the effect of micro polar parameter m. Other parameters are taken as $l = 3$, $\phi = 0.7$, $\omega = 0.001$, $b = 0.04$, $N = 0.20$.

Unlike the wave amplitude dilation parameter ω, the gradient parameter b adversely affects the growth of wall shear stress. Wall shear stress always decreases with increasing gradient parameter [Figure 6.8].

6.4.2 Divergence limited to a small length near the other end

In the previous section we discussed the flow dynamics when the tube diverges throughout. Now we shall examine similar values for a bit different situation, i.e., the tube does not diverge from the beginning. The change in cross sectional area is confined to the other end of the tube to model bulging at the end.

Parametric values are kept the same for the investigation with the only change that the last one third of the tube diverges [Figure 6.9]. The gradient parameter b is varied. $b = 0.0$ corresponds to a uniform tube. Pressure distribution along the tube axis all through the flow reveals similarity with the situation when

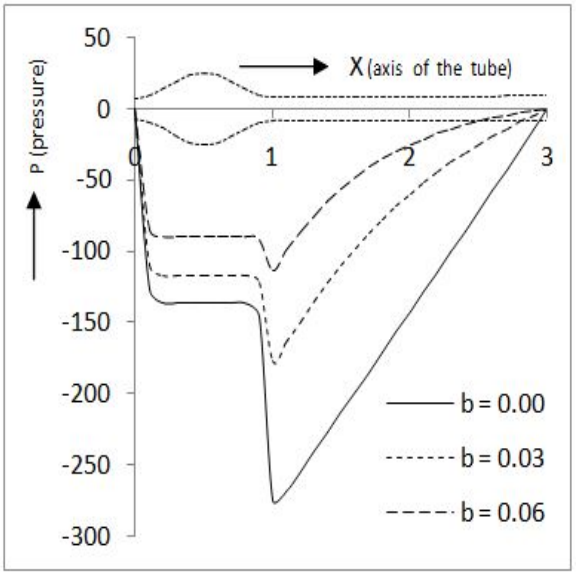

(6.6a) $t = 0.00$

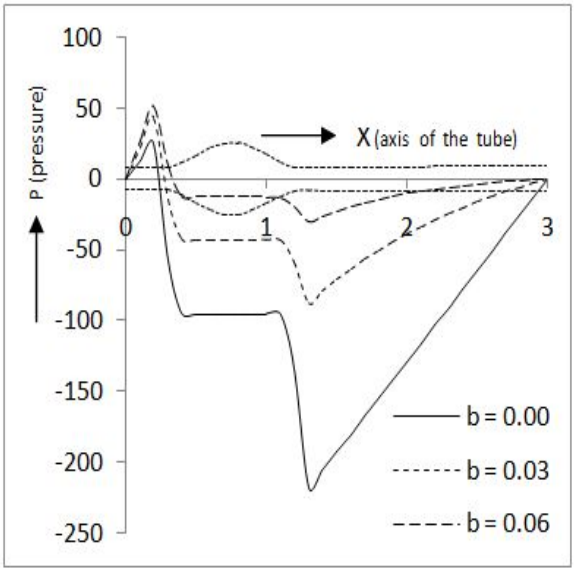

(6.6b) $t = 0.25$

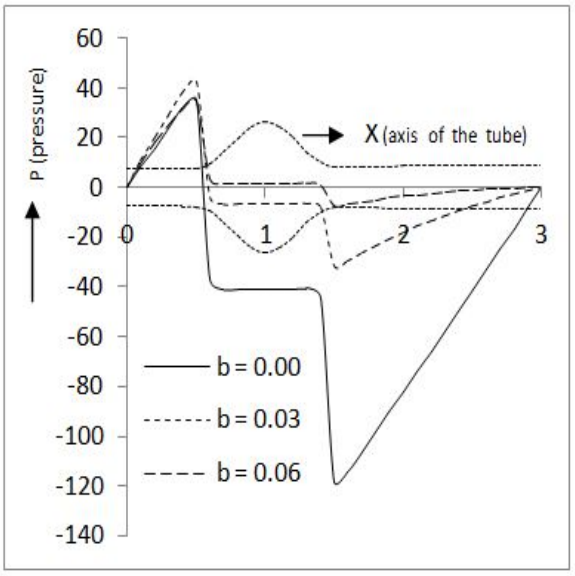

(6.6c) $t = 0.50$

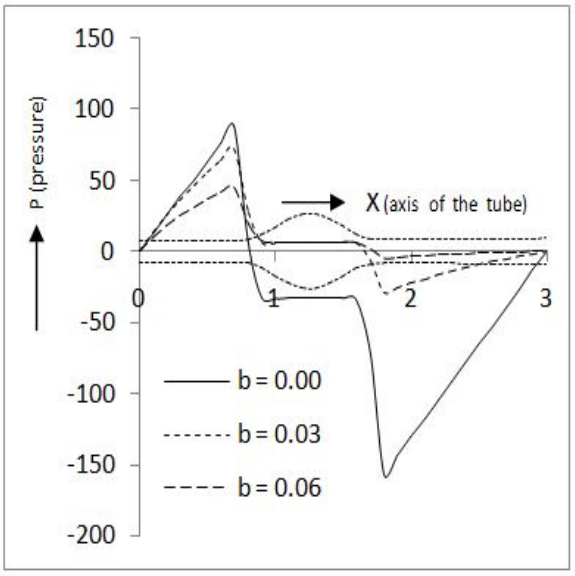

(6.6d) $t = 0.75$

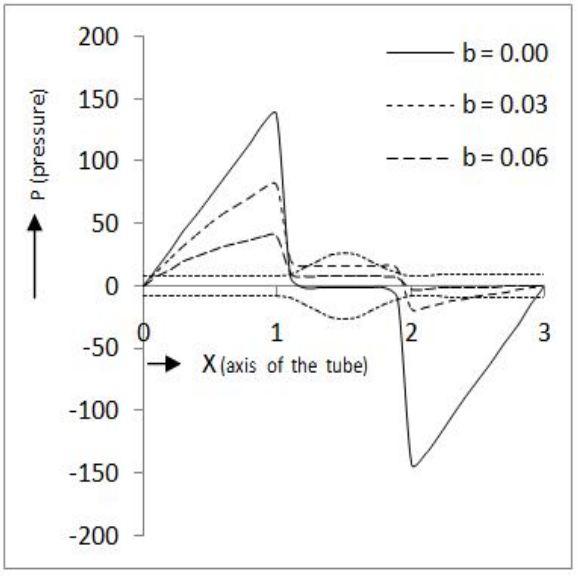

(6.6e) $t = 1.00$

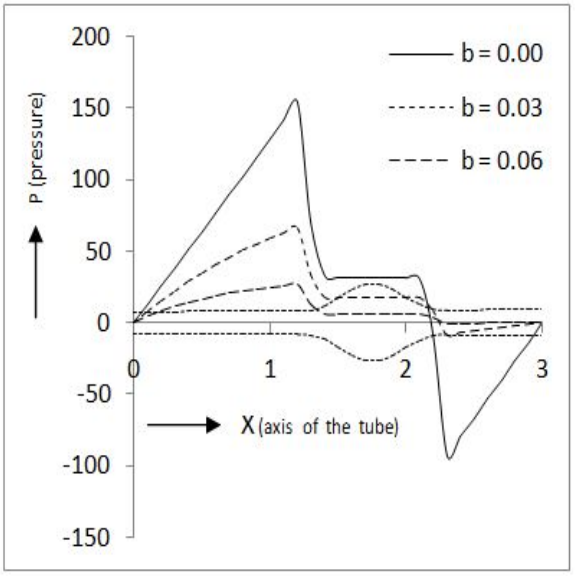

(6.6f) $t = 1.25$

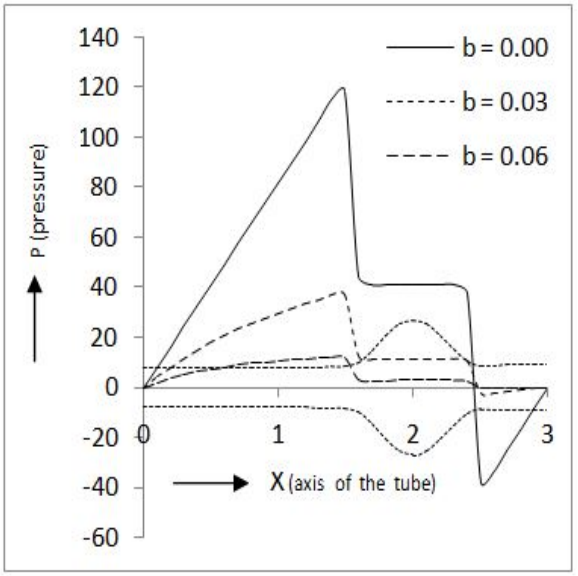

(6.6g) $t = 1.50$

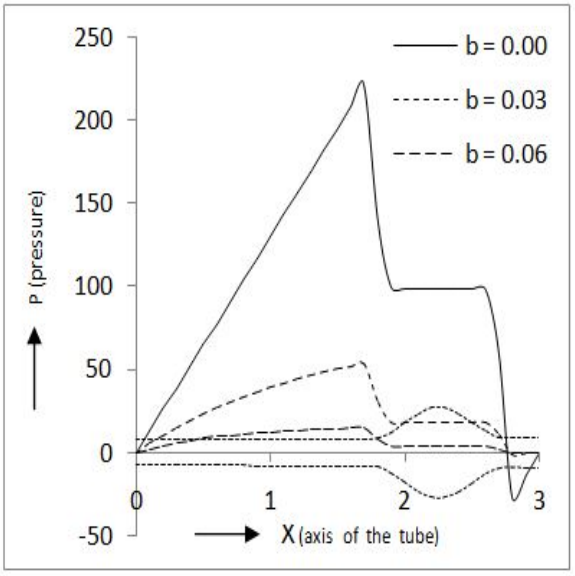

(6.6h) $t = 1.75$

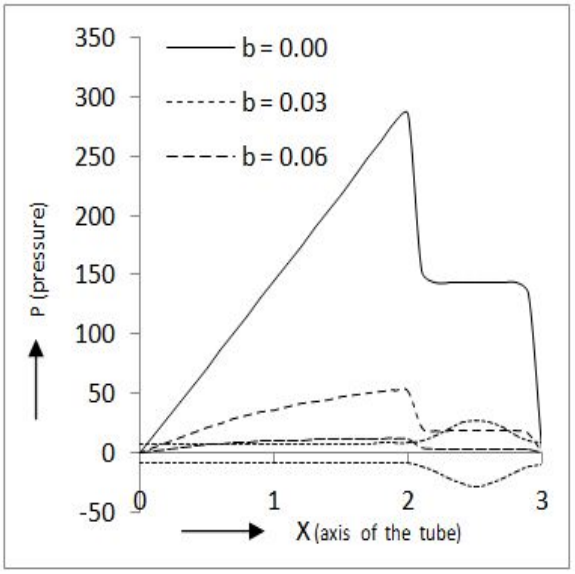

(6.6i) $t = 2.00$

Figure 6.6: Pressure distribution along axial distance at different time instant showing the effect of gradient parameter b. Other parameters are taken as $l = 3$, $\phi = 0.7$, $\omega = 0.001$, $N = 0.20$, $m = 1.00$.

the tube diverged from the beginning. It is to be noted that the fall of pressure did not wait to start where divergence begins but it starts falling right from the beginning even when the tube diverges much later.

6.4.3 Effect of wave amplitude dilation on reflux

Impact of dilating wave amplitude on reflux is an important aspect of investigation. For the micropolar fluids, we fix parameters other than the wave amplitude dilation parameter ω as $N = 0.20, m = 1.0, b = 0.002$, while ω is varied in the range $0.0 - 0.6$. It is observed in Figure 6.10 that the reflux region shrinks if ω increases. One cam conclude from this that wave amplitude dilation opposes reflux even if the fluid is of micropolar nature.

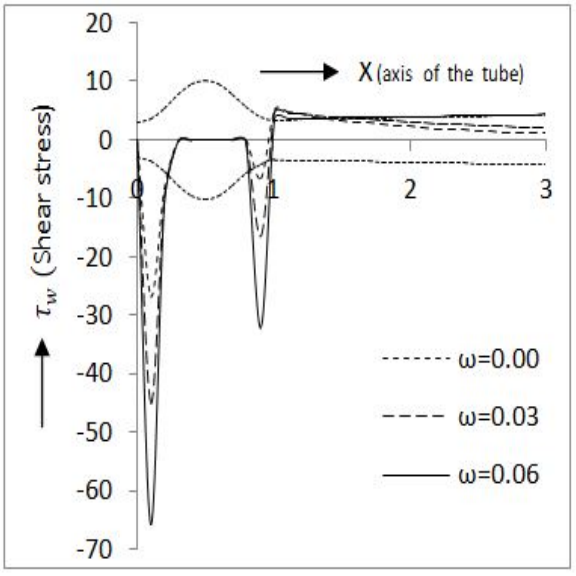

(6.7a) $t = 0.00$

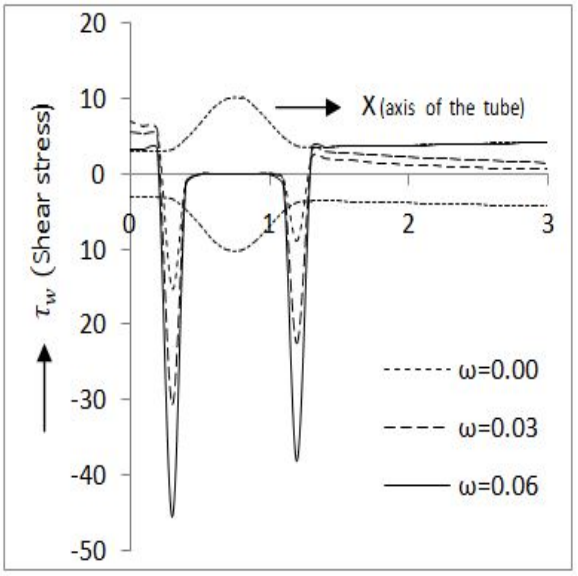

(6.7b) $t = 0.25$

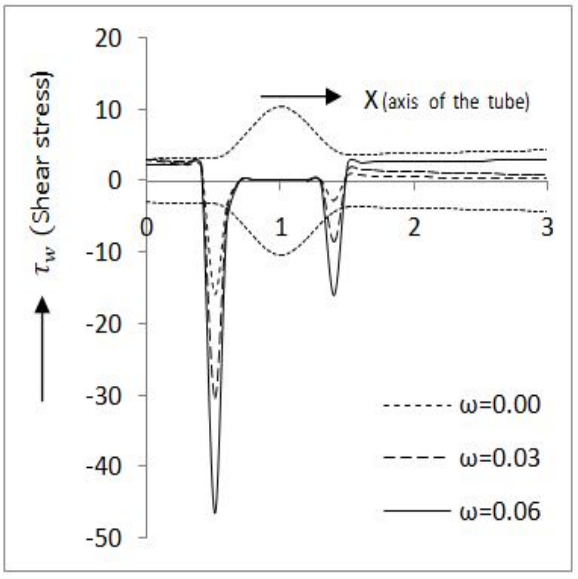

(6.7c) $t = 0.50$

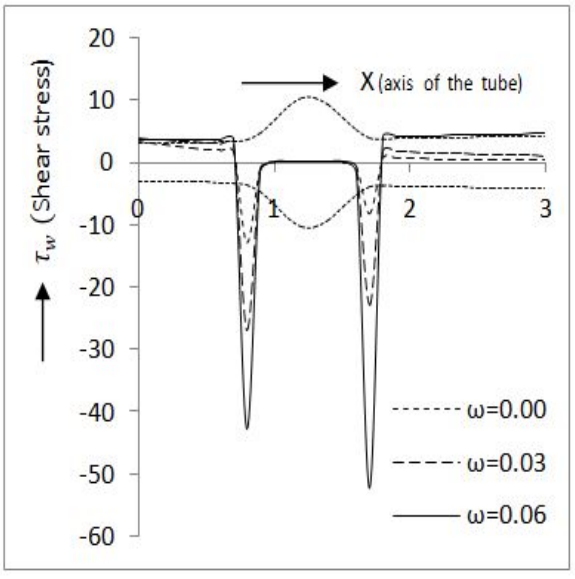

(6.7d) $t = 0.75$

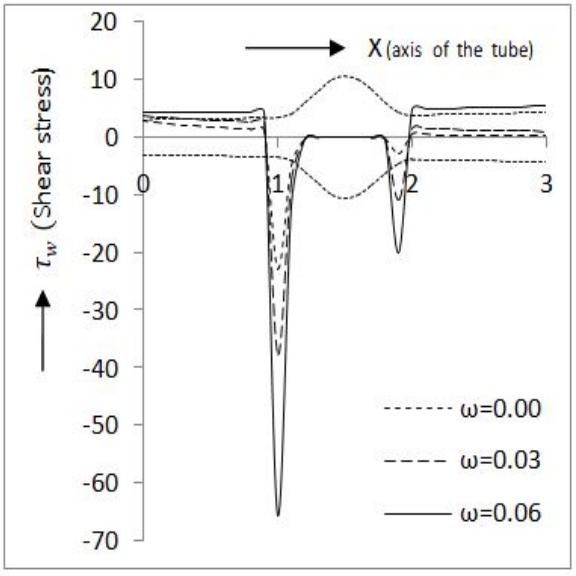

(6.7e) $t = 1.00$

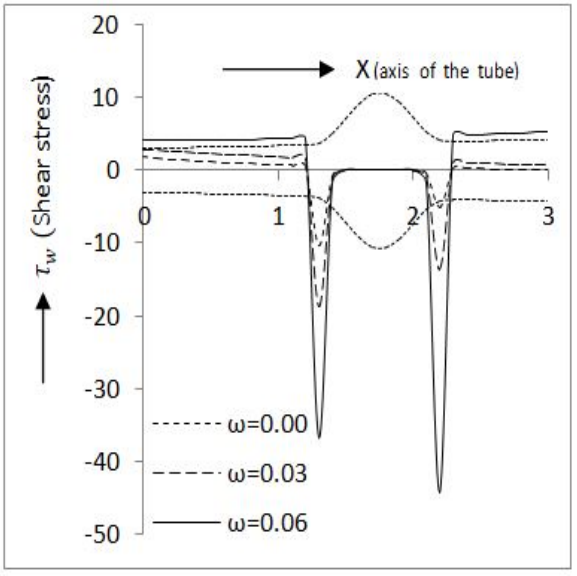

(6.7f) $t = 1.25$

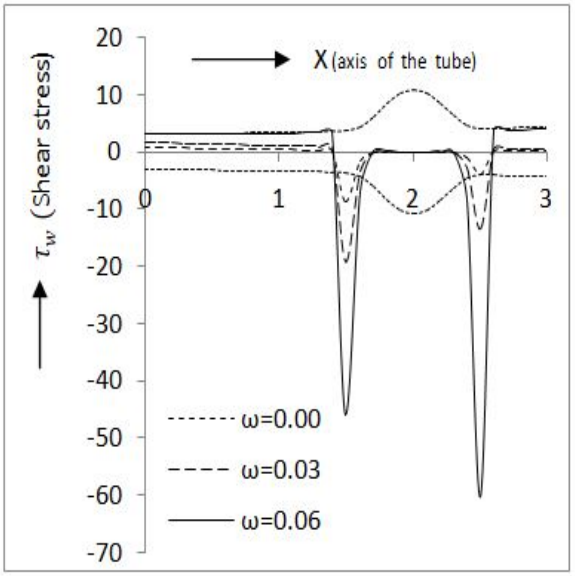

(6.7g) $t = 1.50$

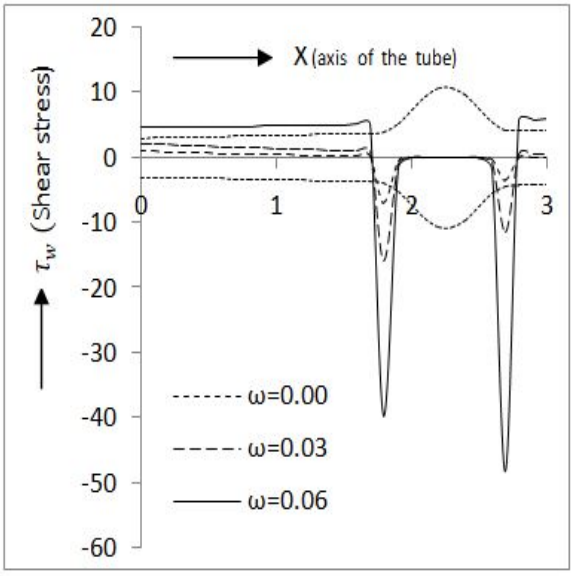

(6.7h) $t = 1.75$

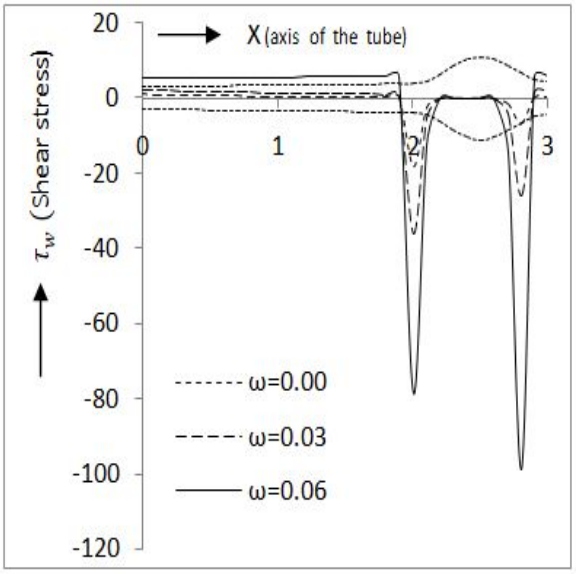

(6.7i) $t = 2.00$

Figure 6.7: Wall shear stress τ_w distribution along axial distance at different time instant showing the effect of dilation parameter ω. Other parameters are taken as $l = 3,\ \phi = 0.7,\ N = 0.20,\ b = 0.04,\ m = 1.0$.

6.5 Conclusion and physical interpretations

The main objective of this analysis is to discover the impact of deformation of oesophagus swallowing a micro polar fluid. This has been attempted by modelling the flow of a micro-polar fluid in a tube of circular cross section which diverges near the other end. Here, the non-Newtonian nature is characterized by the micro-polar parameter and the coupling number. All these characteristics put together give it the micro-polar nature.

From the computational work of the constructed model depicted in plots through observations and discussions in the previous section, we conclude the following:

• Wave amplitude dilation increases pressure all through swallowing process: but divergence in the tube, and hence in herniation in the oesophagus,

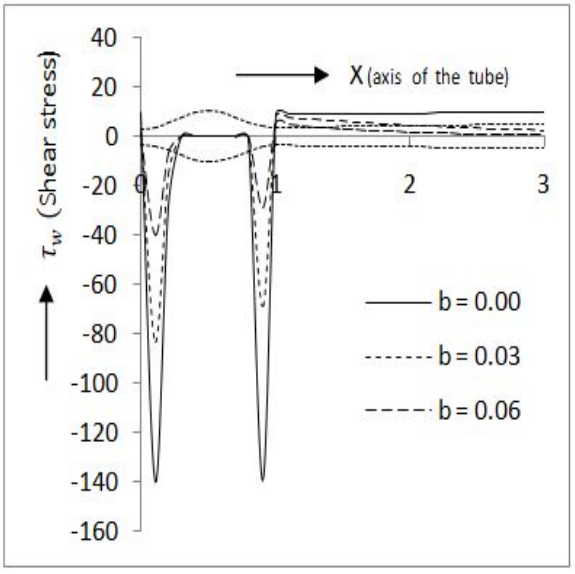

(6.8a) $t = 0.00$

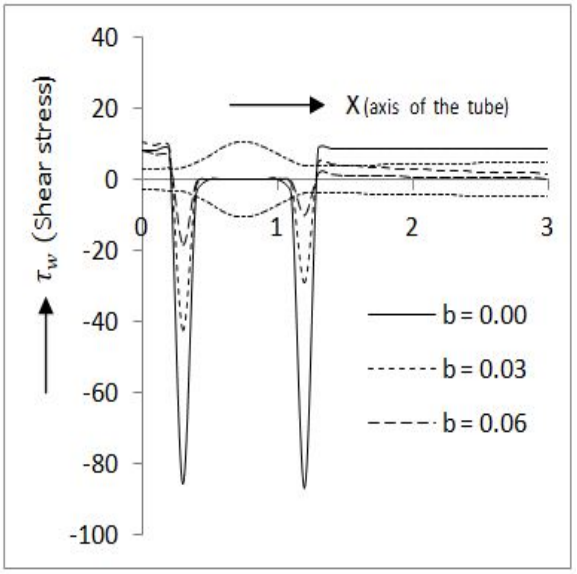

(6.8b) $t = 0.25$

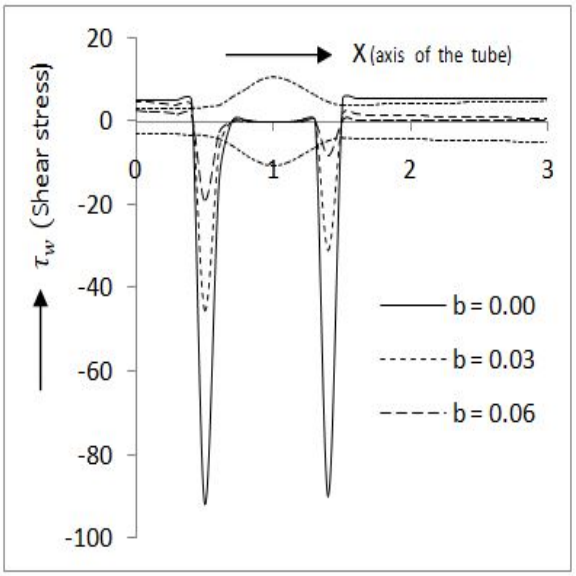

(6.8c) $t = 0.50$

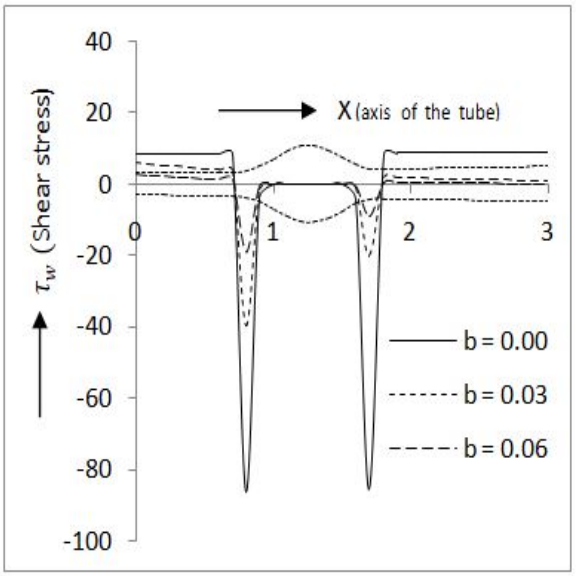

(6.8d) $t = 0.75$

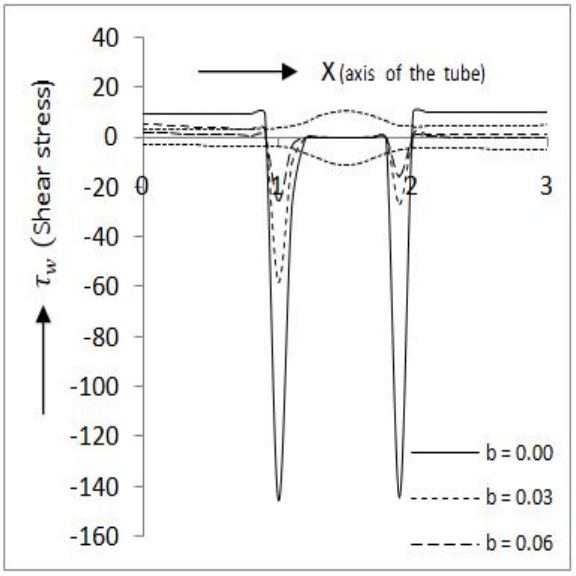

(6.8e) $t = 1.00$

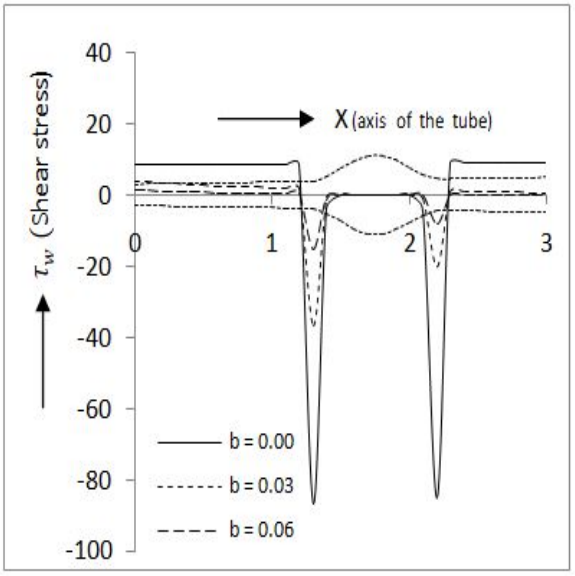

(6.8f) $t = 1.25$

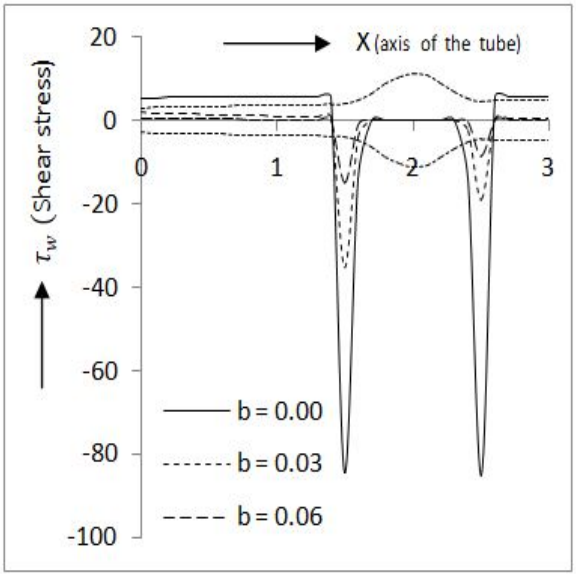

(6.8g) $t = 1.50$

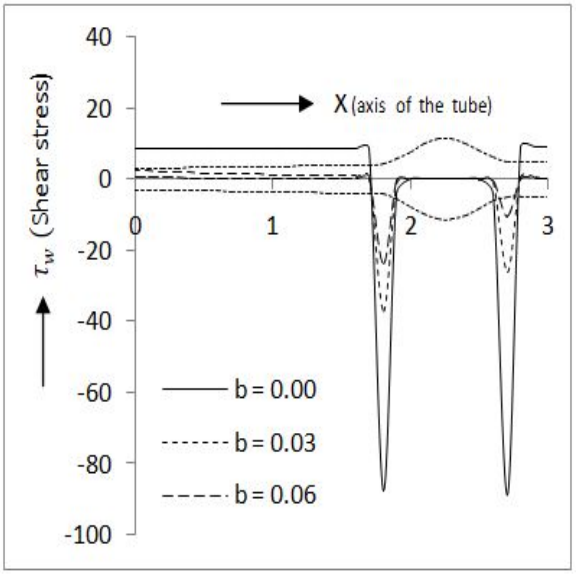

(6.8h) $t = 1.75$

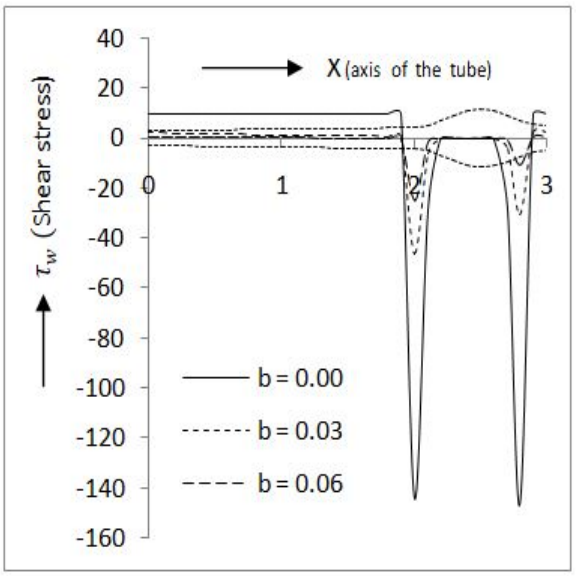

(6.8i) $t = 2.00$

Figure 6.8: Wall shear stress τ_w distribution along axial distance at different time instant showing the effect of gradient parameter b. Other parameters are taken as $l = 3,\ \phi = 0.7,\ N = 0.20,\ m = 1.0$.

uniformly decreases pressure.

• This is true when divergence is either throughout the length, or confined to a small length near the distal end.

• This reveals that less pressure is enough to carry the same bolus into the stomach in case the tube diverges fully or partly above the hiatus.

• The physical interpretation is that the patient has no difficulty in swallowing so long this deformation is limited to sliding hiatus hernia which is a mild hernia.

• Exponential bulging, which is a new assumption close to natural bulging in oesophagus, makes swallowing further easier.

• This indicates the dysfunction may go unnoticed. However, heart burn etc. will certainly indicate.

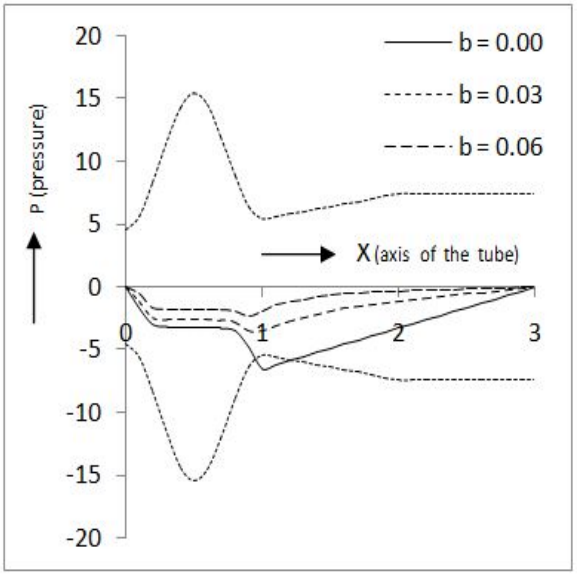

(6.9a) $t = 0.00$

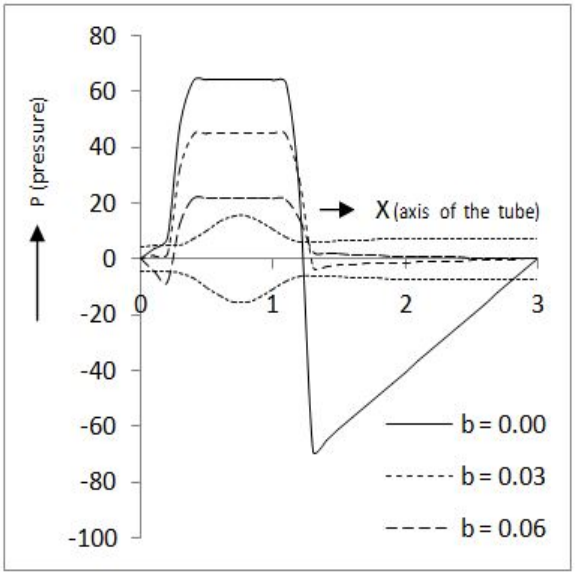

(6.9b) $t = 0.25$

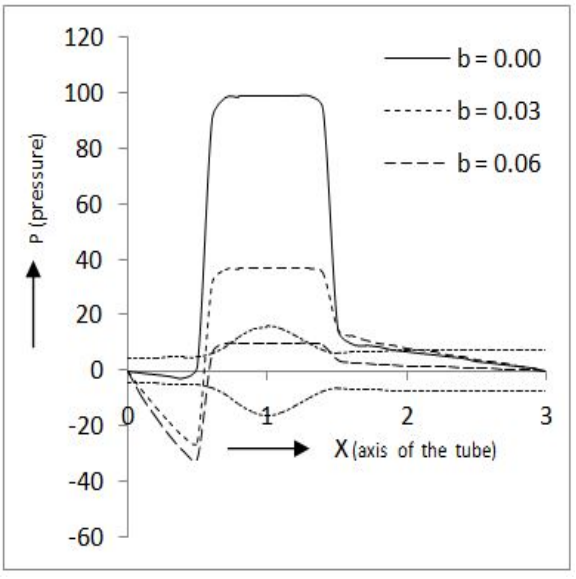

(6.9c) $t = 0.50$

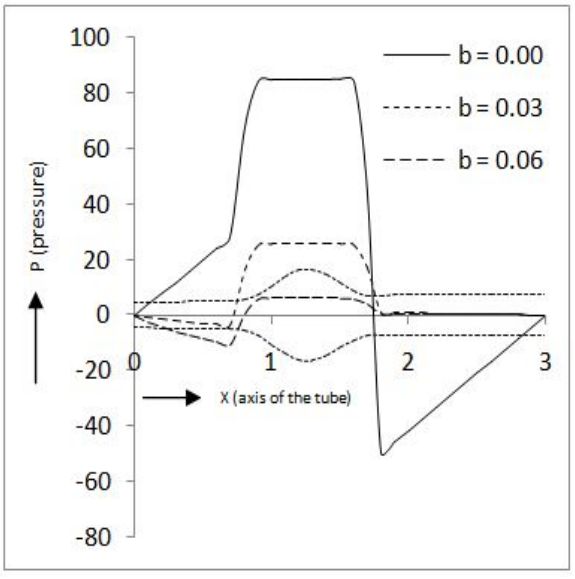

(6.9d) $t = 0.75$

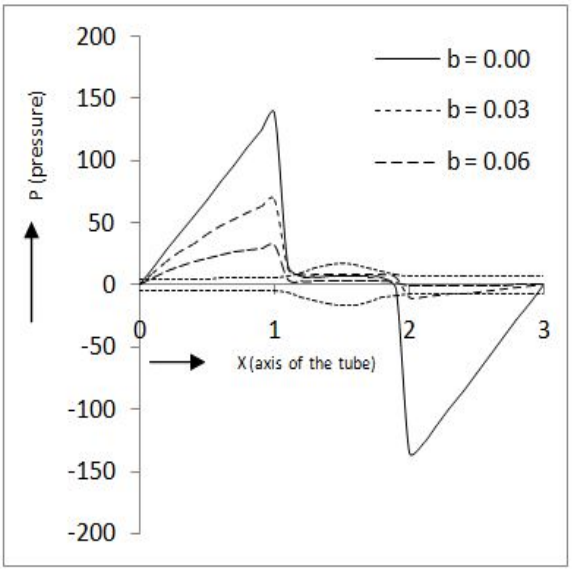

(6.9e) $t = 1.00$

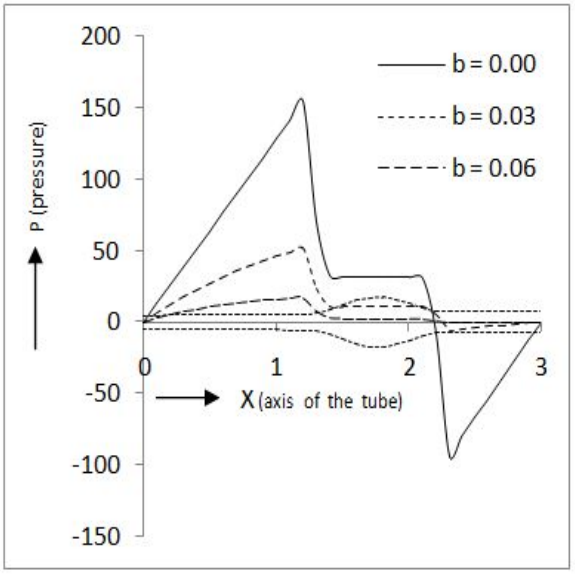

(6.9f) $t = 1.25$

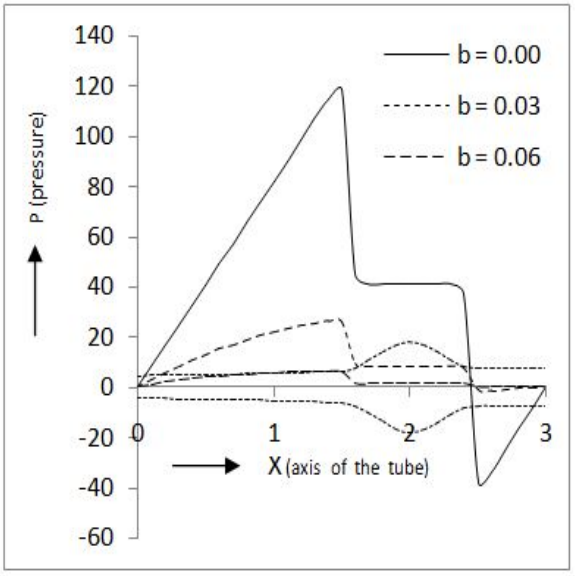

(6.9g) $t = 1.50$

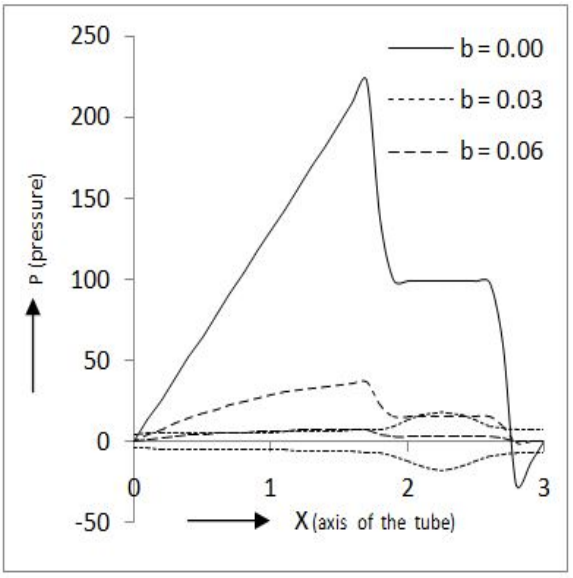

(6.9h) $t = 1.75$

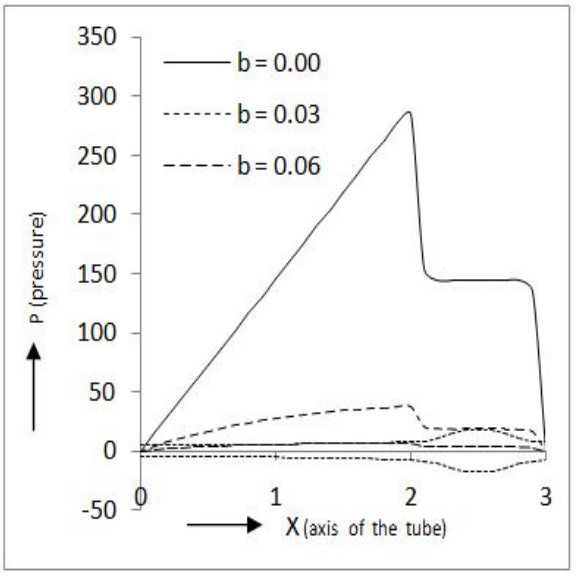

(6.9i) $t = 2.00$

Figure 6.9: Pressure variation along the length of oesophagus at different time instants showing the effect of gradient parameter b when tube diverges at distal end. Other parameters are taken as $l = 3$, $\phi = 0.7$, $N = 0.20$, $m = 1.0$.

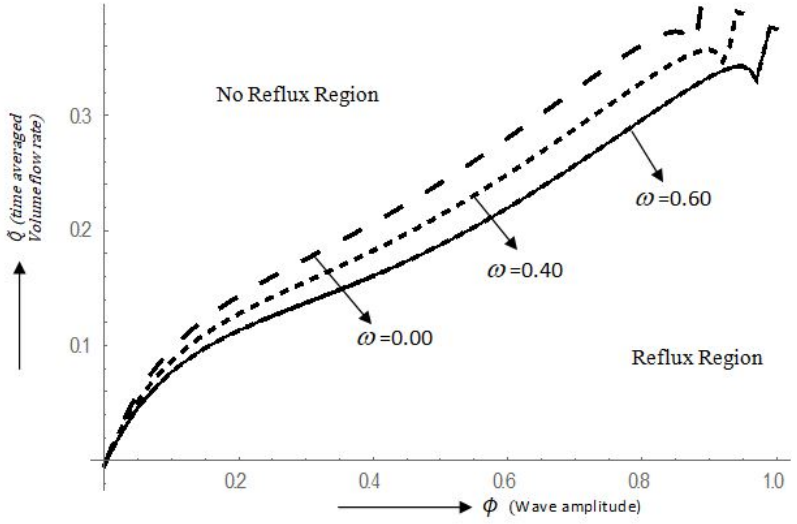

Figure 6.10: The diagram exhibits the relation between time averaged flow rate $\bar{Q}$ and wave amplitude ϕ showing the effect of dilation parameter ω. Other parameters are taken as $N = 0.20$, $m = 1.0$, $b = 0.002$.

• The non-dimensional parameters have opposing impacts. An increase in coupling number requires more pressure to be exerted by the oesophagus wall on the fluid swallowing inside it whereas the micro-polar parameter shows an opposite tendency.

• While the wave amplitude dilation parameter favours wall shear stress, the gradient parameter which causes divergence if cross section of the tube, adversely affects the growth of wall shear stress. Wall shear stress always decreases with increasing gradient parameter.

• It is further inferred that dilating wave amplitude dilation causes the flow to be less prone to reflux.

****